4

Interplay between Tectonics and Mount Etna's Volcanism: Insights into the Geometry of the Plumbing System

Domenico Patanè et al.*
Istituto Nazionale di Geofisica e Vulcanologia,
Sezione di Catania – Osservatorio Etneo, Catania
Italy

1. Introduction

Volcanoes are geologic manifestations of highly dynamic and complexly coupled physical and chemical processes in the interior of the Earth. Most volcanism on Earth occurs at plate boundaries in places where tectonic plates move apart (e.g. Iceland) and in places where tectonic plates come together with one plate plunging (subducting) below the other into the mantle (e.g. Pacific ring of fire). Conversely, intraplate volcanism is a type of volcanism occurring far from plate boundaries and whose origins are rather controversial.
To know the working mode of a volcano in a given region it is necessary to understand the interplay between tectonics, deformation processes and magma transport through the lithosphere (e.g. Vigneresse, 1999; Petford et al., 2000). Deformation-induced fault-fracture networks have been regarded as efficient pathways through which magma is transported, stored and eventually erupted at the Earth's surface (e.g. Clemens and Mawer, 1992; Petford et al., 2000). At active volcanoes, magmas rise toward the surface and can stagnate at different levels in the lithosphere, giving rise to magma bodies of different shape and size (Marsh, 2000). Nearly all volcanic eruptions are supplied with magma through dykes and inclined sheets whose initiation and eventual propagation to the surface or, alternatively, arrest at some depth in the volcano, depend on the stress state in the volcano (Gudmundsson, 2006). At the surface of active volcanic edifices, the majority of eruptive fissures have a radial configuration and tangential or oblique fissures are rare. However, within many eroded volcanic edifices, dykes and dyke-fed eruptive fissures commonly have more complex patterns, resulting from regional stresses, magmatic reservoirs, anisotropies or variations in topography (Acocella et al., 2009).
Geophysics can provide information on the geometry of plumbing system and magma chambers, as well as on the mechanisms of emplacement of dykes. Among the different branches of geophysics, seismology is the most powerful tool to obtain information about

* Marco Aliotta, Andrea Cannata, Carmelo Cassisi, Mauro Coltelli, Giuseppe Di Grazia, Placido Montalto and Luciano Zuccarello
Istituto Nazionale di Geofisica e Vulcanologia, Sezione di Catania – Osservatorio Etneo, Catania
Italy

the inner structure of volcanoes and the geometry of their plumbing systems. Volcanoes generate seismic energy at frequencies ranging from zero (static displacement) to a few tens of Hz. Generally, two different groups of seismic signals can be distinguished in volcanic areas (Chouet, 1996): the former, involving processes originating in the solid, is associated with shear failures in the volcanic edifice and the related seismic events are called volcano-tectonic (VT) earthquakes; the latter (hereafter referred to as seismo-volcanic signals) involves processes originating in the fluid and includes long-period (LP) events and volcanic tremor, sharing the same spectral components (0.5-5 Hz), and very-long-period (VLP) events characterized by dominant period of 2-100 s (Ohminato et al., 1998).
In the last 30 years, the Earth has been widely investigated through a variety of seismic tomographic methods, leading to many interesting results at both regional and global scale. In volcanic environments, several tomographic high-resolution studies, involving the joint use of local VT earthquakes and artificial explosions have led to important discoveries on volcano plumbing systems both in the shallow and deeper zones (e.g. Achauer et al., 1988; Lees and Crosson, 1990). It is noteworthy that, since the ability to resolve feeding conduits, magma chambers, and zones of solidified magmatic intrusion relies on both the distribution of elastic sources at depth and of receivers at the surface, objects smaller than a few km generally cannot be reliably resolved. In this sense, what we can define with seismic tomography is generally a "large" volcanic structure with minimum dimensions of 1-3 km^3. Smaller structure composing the shallow portion of the plumbing system can be studied by volcanic tremor and LP and VLP events, which, as aforementioned, are driven by fluid processes. The study of these signals can provide information not only on the geometry of the shallow portion of the plumbing system, but also on the variations in time of the magma batches stored inside it (Chouet, 2003).
This chapter deals with the investigation of the plumbing system at Mt. Etna by using seismic signals with the aim of understanding how Etna volcano structure works and its relationship with the geodynamics of eastern Sicily. In particular, **section 2** summarizes the main structural features of Mt. Etna, some theories regarding its origin, as well as some information about the volcano's recent activity. **Section 3** focuses on the investigation of the deep plumbing system by seismic tomography reporting also the previous seismological studies. In **section 4** examples of study of the shallow plumbing system by the analyses of the seismo-volcanic signals are shown. Finally, **section 5** summarizes the main conclusions.

2. Tectonic setting of Mt. Etna volcano

Mt. Etna is one of the most active volcanoes in the world, located on the densely inhabited eastern coast of Sicily (Italy). It is characterized by almost continuous eruptive activity from its summit craters and fairly frequent lava flow eruptions from fissures opened up on its flanks. Mt. Etna is a composite, quaternary, basaltic volcano set in a region of complex geodynamics, where major regional structural lineaments play an important role in the dynamic processes of the volcano (e.g. Gresta et al., 1998; **Fig. 1**). It covers an area of about 1,250 km^2 with a basal circumference of 140 km and reaches a maximum elevation of 3330 m. On the volcano summit four active craters are currently opened: Voragine, Bocca Nuova, South East Crater, and North East Crater (hereafter referred to as VOR, BN, SEC and NEC, respectively; **Fig. 2**).

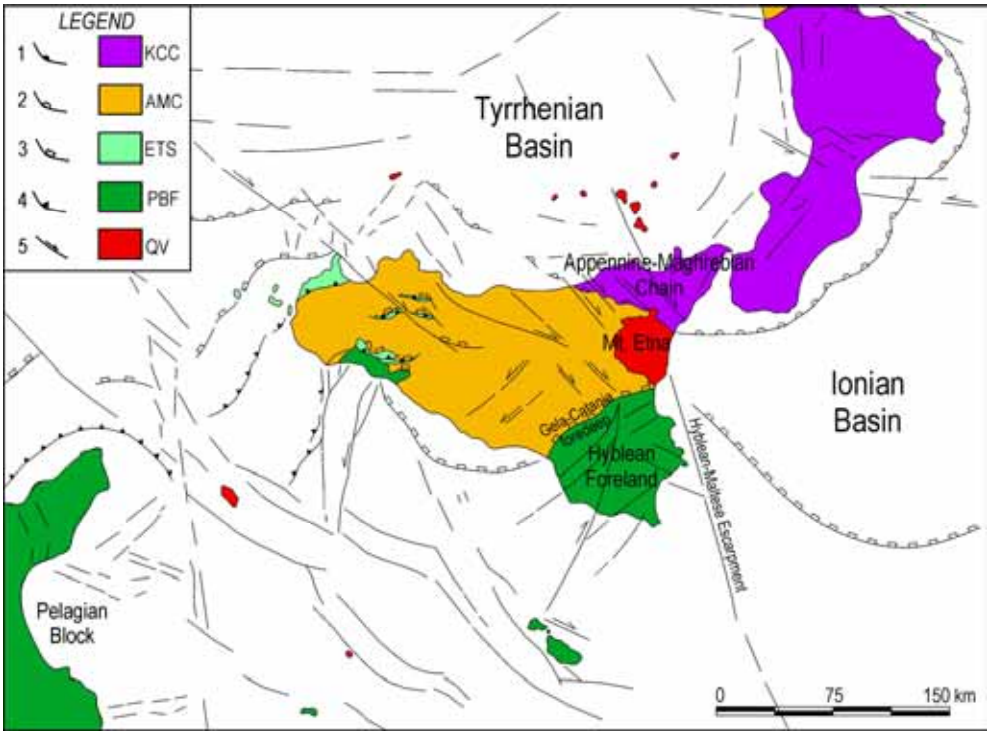

Fig. 1. Structural setting of central Mediterranean Sea (modified from Lentini et al., 2006) and location of Mt. Etna. 1) Regional overthrust of the Sardinia-Corsica block upon Calabride units; 2) Regional overthrust of the Kabilo-Calabride units upon the Apennine-Maghrebian Chain; 3) External front of the Apennine-Maghrebian Chain upon the Foreland units and the External Thrust System; 4) Thrust front of the External Thrust System; 5) Main normal and strike-slip faults. KCC: Kabilo-Calabride Chain Units; AMC: Appennine-Maghrebian Chain Units; ETF: External Thrust System Units; PBF: Pelagian Block Foreland Units; QV: Quaternary Volcanoes. Redrawn from Lentini et al. (2006)

2.1 Structural framework

Mt. Etna lies on the Sicilian continental crust and is located on the external boundary of the Apennine-Maghrebian chain, close to the Gela–Catania Plio-Quaternary foredeep (Bousquet and Lanzafame, 2004). It is bordered by three tectonic domains (**Fig. 1**): the Apennine-Maghrebian Chain northward and westward; the Hyblean Foreland southward belonging to the Pelagian Block, the northernmost part of the African plate (Lentini et al., 2006); the Ionian Basin eastward, an oceanic basin opened during the middle-late Mesozoic and aborted during the Tertiary (Catalano et al., 2001). The thickness of the crust of eastern Sicily has recently been reinterpreted (Cernobori et al., 1996; Continisio et al., 1997; Hirn et al., 1997; Nicolich et al., 2000) allowing the crustal structure in eastern Sicily and the Moho topography beneath the Ionian Sea to be better defined. The Moho has been located at a depth of 30 km beneath the central Hyblean Plateau, rising to 22 km in the Gela-Catania foredeep and to 21–18 km just offshore Catania (Nicolich et al., 2000).

Mt. Etna is sited in an anomalous external position with respect to the arc magmatism and back-arc spreading zones associated with Apennines subduction (Doglioni et al., 2001).

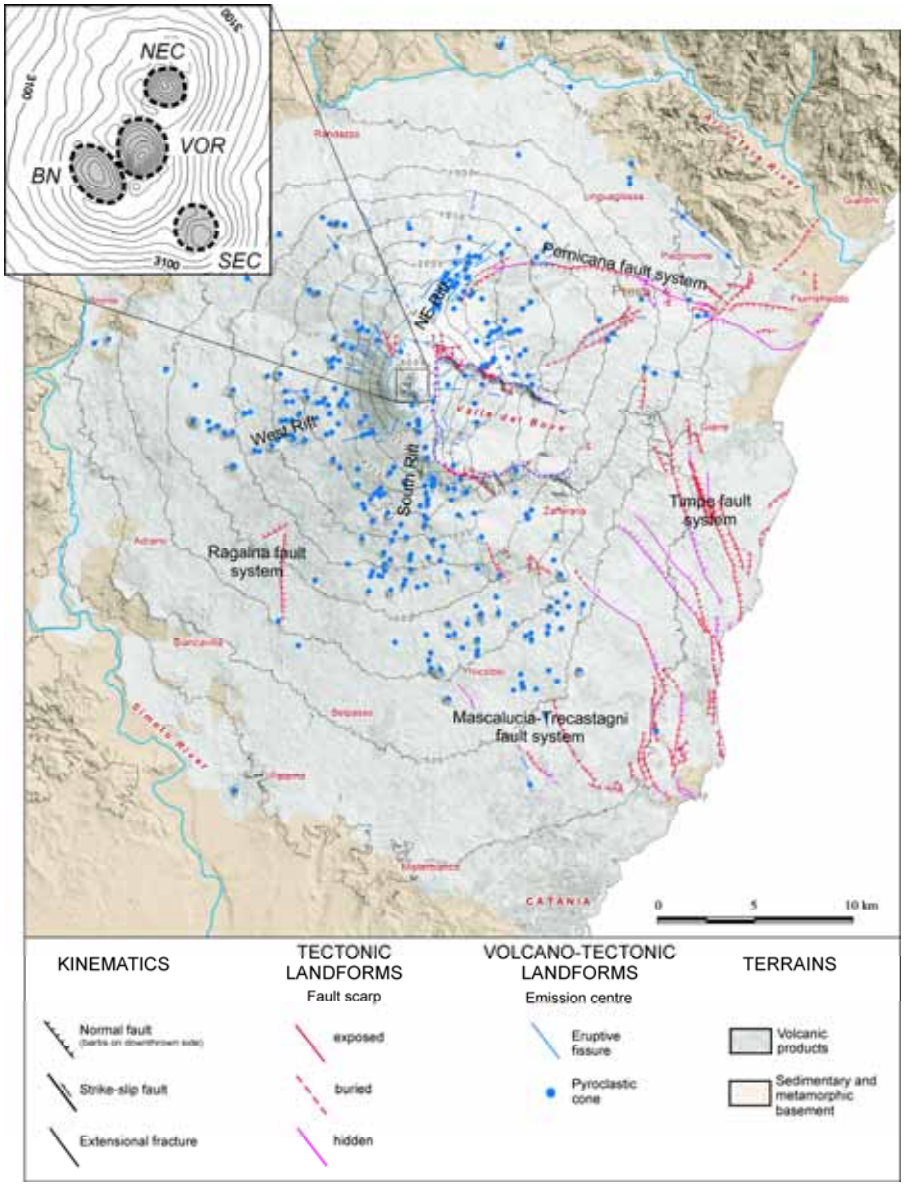

Fig. 2. Structural map of Mt. Etna with the location of the main fault and fissure systems. The location of the summit craters is shown in the inset in the upper left corner (VOR = Voragine, BN = Bocca Nuova, SEC = South-East Crater, NEC = North-East Crater). Redrawn from Azzaro et al (in press)

The structural features of Mt. Etna appear rather complex. On the volcano surface different fault and fissure systems can be recognized (**Fig. 2**). The most outstanding tectonic features at Mt Etna are clearly recognizable on the east and south-east flanks of the volcano, where the clearest morphological evidence of active faulting exists (**Fig. 2**). Here, seismogenic faults can be related to the NNW–SSE Malta Escarpment that is the main lithospheric structure in the eastern Sicily. Other seismogenetic faults (Patanè et al., 2005), though not recognizable on the surface, can be linked to the NE–SW, ENE–WSW fault systems that control the tectonic evolution of the northern margin of the Hyblean Plateau (Torelli et al., 1998). The eastern flank of Mt. Etna is characterized by frequent shallow seismic activity (depth <7 km) and by a seismic creep along some faults. Conversely, the western flank of Mt Etna, normally characterized by a deeper seismicity (depth >5 km), is considered the most stable sector of the volcano. In the western sector, there is only slight morphological evidence of faulting, such as some short segments of faults observable on the south-western flank (e.g. Ragalna fault). However, it must be noted that the faults with morphological evidence may represent only a part of the tectonic structures present in the Etnean area and hidden fault segments could be covered by the huge pile of volcanic products (e.g. Azzaro, 1999).

Following, some of the main tectonic features are discussed:

Timpe fault system. The normal faults belonging to this system dip toward the Ionian Sea and represent the most outstanding structural feature of the volcano. They displace a large part of the eastern flank by a 20 km long and 5 km wide belt of mainly extensional structures, striking from N to NW. Running from the coast to the south toward the inner volcano slope to the north, the fault system consists of a series of parallel seaward-facing step-faults segmented into individual steep fault escarpments up to 8 km long and up to 200 m high, that offset late Pleistocene to Holocene volcanics and historical lava flows. Acireale fault to the south and Moscarello fault to the north, represent the main elements of the Timpe fault system, and the N-S trending S. Alfio fault represents its northernmost apex. Timpe fault system is associated with shallow-depth (<7 km) seismicity including the occurrence of several earthquakes with M equal to 4.5 (Azzaro et al., 2000).

Pernicana fault system. It is located in the north-eastern flank of the volcano, trends E-W and can be considered the most active fault in the Etnean area, as testified by the slip rate estimations and geodetic measurements (up to 2.8 cm/y; Rasà et al., 1996; Neri et al., 2004; Bonforte et al., 2011). This system develops eastward from the NE rift (from 1850 m a.s.l.) to the coastline, over a distance of about 20 km. The westernmost part is mainly characterized by normal dip-slip motion, whereas the easternmost one by left strike-slip motion. The Pernicana fault system is partially characterized by a scarp with a maximum morphological height of 70-80 m between 1000 and 1500 m a.s.l. At lower elevations (starting from 800 to 700 m a.s.l.) this system has a less defined morphological expression (Acocella and Neri, 2005). Despite its continuity, Pernicana can be roughly divided into two main portions (western and eastern), characterized by differential times and amounts of displacement as evidenced during the 2002-2003 eruption (Neri et al., 2004). The western Pernicana, about 11 km long (from the NE Rift to Presa), shows the larger displacement even though the long-term slip rates are similar in both portions. Moreover, the western portion is associated with shallow (< 2-3 km) and moderate seismic activity (2<M<3.5; Azzaro et al., 1998). The eastern portion, about 9 km long (from Presa to the coastline), is aseismic and was recognized during the 2002-2003 eruption. These different styles of deformation may be due to the different rheological properties of their substratum (Neri et al., 2004).

Mascalucia-Trecastagni fault system. It is located in the southeastern flank and is composed of NNW-SSE-striking faults displaying prominent linear scarps near the towns of Mascalucia and Trecastagni (Azzaro, 2004). It is mainly characterized by strike-slip motion and by shallow seismicity, with focal depth of 1-2 km (Lo Giudice and Rasà, 1992).
Ragalna fault system. It is located in the southwestern flank of the volcano and comprises two linked structures, the main one extending for as much as 5 km in a roughly N direction towards the summit area of the volcano (Rust and Neri, 1996; Azzaro et. al., in press). Examination of the fault system in the field indicates dominantly dip-slip extensional displacement (Rust and Neri, 1996). The active faults of this system bound a triangular structure like horst (Rust and Neri, 1996).
The volcano is also characterized by a peculiar arrangement of the eruptive fissures that diverge from a radial distribution typical of stratovolcano edifices. The fissures are mainly concentrated on three sectors of the volcano named NE Rift, South Rift and West Rift, as previously indicated by several authors (Kieffer, 1975 and 1985; Lo Giudice et al., 1982; Mcguire and Pullen, 1989; **Fig. 2**).
NE Rift. It is located on the northeastern flank of the volcano and from the summit forms a 5-km-long, 2-km-wide topographic ridge made up of eruptive fissures, pit craters and pyroclastic cones. The swarm of eruptive fissures have dispersion axes ranging from 15°E to 50°E showing a gradual clockwise rotation along the rift towards NE (Tibaldi and Groppelli, 2002). The northeastern flank shows another smaller swarm of fissures and cones from the northern slope of the Valle del Bove, with dispersion axes ranging from 70°E to 90°E and a main ENE trend.
South Rift. The southeastern flank is characterized by a more scattered distribution of the eruptive fissures and cones. Over a 12 km wide sector the dispersion axes of the fissures range from 200°E to 140°E. The main belt of the rift develops between the SEC and the southwestern rim of the Valle del Bove along a SSE direction, and then continues southeastward as the rim swings to an easterly direction. On the southern slope of the volcano it forms a more diffuse set of N-S to SSW-NNE striking fissures extending from the Montagnola area to Nicolosi, at a distance of about 10 km.
West Rift. On the west flank eruptive fissures and cones are more radially distributed, even if a concentration of these elements appear over a 4.5 km wide sector between 245°E and 280°E marking the so-called West Rift characterized by WSW and W main trends of the eruptive axis (Bellotti et al., 2010).

2.2 Geological history and origin of volcanism

According to Branca et al. (2004), the beginning of volcanism in Etnean region is due to the northward migration of the Plio-Pleistocene Hyblean magmatic source. Volcanism began at about 500 ka ago through submarine eruptions on the Gela–Catania foredeep basin. About 300 ka ago fissure-type eruptions occurred on the ancient alluvial plain of the Simeto River forming a lava plateau. From about 220 ka ago, the eruptive activity was localized mainly along the Ionian coast where fissure-type eruptions built a shield volcano. Between 129 and 126 ka ago volcanism shifted westward toward the central portion of the present volcano (Branca et al., 2007). This change caused a variation in the volcanic chemical composition (from subalkaline to purely alkaline) as well as in the type of volcanism, which from fissural became central and shifted westward. The stabilization of the plumbing system marked the beginning of the construction of small polygenic edifices (e.g. Trifoglietto volcano) in Valle

del Bove from 107 ka to 65 ka ago (De Beni et al., in press). About 57 ka ago, another westward shift of the plumbing system started the building of the stratovolcano (De Beni et al., in press) that represents the main bulk of the Mt. Etna edifice. This volcanic center reached its maximum areal expansion about 40 ka ago, proceeding up to 15 ka when four plinian eruptions formed a large summit caldera, historically named Ellittico Crater (Coltelli et al., 2000). The final evolution of this process took place during the Holocene, when eruptive activity resumed inside the caldera and expanded outside to cover the previous Ellittico edifice forming the volcanic succession of the present active volcanic center (Branca et al., 2004).

The complex geological history and tectonic setting of Mt. Etna have given rise to a great number of models to interpret its origin and the peculiar features for a very active basaltic volcano that is so unusually located in front of an active thrust belt:

- Rittmann (1973) interpreted the intersection of three main fault systems, trending ENE, NNW and WNW, as the mechanism that created a weakness zone for magma uprising.
- Tanguy et al. (1997) proposed how the upwelling of the asthenosphere first caused extensive melting of a mantle diaper, allowing tholeitic magma to accumulate near the mantle-crust interface. Then, increasingly alkaline basalt was generated and fed the entire volcanism of Mt. Etna by undergoing continuous but limited differentiation in a subcrustal reservoir.
- Monaco et al. (1997) infer that the magmatism at Mt. Etna can be related to the dilatational strain on the footwall of an east-facing, crustal scale normal fault located along the Ionian shore. In fact, on the basis of structural, seismological and volcanological studies of 2001 and 2002-2003 eruptions, Monaco et al. (2005) state that the conditions of magma ascent are strongly dominated by extensional structures related to this dilatational strain.
- Gvirtzman and Nur (1999) advanced the idea of the "suction" of asthenospheric material from under the neighboring African plate to cause the voluminous melting under Mt. Etna. Such lateral flow is expected when descending slabs migrate backwards in the mantle. A similar model was also developed by Doglioni et al. (2001). According to these Authors, the right lateral transfer along the Malta escarpment is a transtensional "window" between the Sicilian and Ionian segments of the Apennines slab.
- According to some Authors, Mt Etna's magmatism is related to the instability of the eastern flank of the volcano. Indeed, deformation measurements carried out by GPS, SAR and so on, suggest that the eastern flank of the volcano is sliding toward the sea (e.g. Froger et al., 2001; Lundgren et al., 2003; Palano et al., 2008). Some authors believe this sliding motion may cause the decompression of the plumbing system, facilitating the uprise of magma to the surface (Branca et al, 2003; Neri et al., 2004). The location of the sliding surface is open to debate. Lo Giudice and Rasà (1992) postulate a shallow slip surface (0-1 km a.s.l.) consistent with the very shallow seismicity (depth < 1.5 km). Borgia et al. (1992) and Rust and Neri (1996) suggest a detachment as deep as about 5 km occurring within weak sediments of the Gela-Catania Foredeep. Bousquet and Lanzafame (2001) envisage a decollement between the volcanic pile and the sedimentary substratum (1-2 km a.s.l.). Finally, Tibaldi and Groppelli (2002) suggest that both a shallow and a deep decollement surface can characterise, at the same time, the eastward sliding of the volcano. The unstable zone is confined by the Pernicana

fault to the northwest, by the NE rift and the fissure systems in the summit area, and by the Ragalna fault system to the southwest. The Trecastagni-Mascalucia fault system is likely originated by differential movements within the collapsing sector of the volcano (Rust and Neri, 1996).

- Chiocci et al. (2011), by studying the marine geological and geophysical data of the continental margin facing the volcano, found a large bulge offsetting the margin that is deeply affected by widespread semicircular steps, interpreted as evidence of large-scale gravitational instability. Such features extend inshore to the mobile eastern flank where the larger ground deformations are measured. Both submarine instability and subaerial flank sliding are bounded by two regional tectonic lineaments to accommodate the basinward movement of this large sector of the continental margin topped by the Etna volcanic pile. The Authors infer that the instability process involving the Sicilian continental margin facing Etna volcano during the last 0.1 Ma may be considered a very large mass-wasting phenomenon. This is due to the magmatic intrusion rather than any tectonic process related to a late-orogenic phase of the Apennine Chain thrusting this portion of the continental margin. Indeed, the bulge has no trace of any compressive structures, as previously expected by Borgia et al. (1992) and Rust et al. (2005). Conversely, it is pervaded by extensional and transtensional structures representing the brittle response to a large-scale and long-lasting gravitational instability affecting the continental margin. This model implies that an extensional tectonics induced by the sliding of the volcano eastern flank has been acting continuously over the last 0.1 Ma since the bulge collapse effects are propagating upslope. The continuous decompression at the volcano summit favors the ascent of basic magma without lengthy storage in the upper crust, as one might expect in a compressive tectonic regime. This may be the cause or one of the main contributory causes of the growth of a very active basaltic volcano on top of such an active thrust belt as the Apennine Chain in Sicily.

2.3 The recent volcanic activity since 2000

Two main types of volcanic activity may be distinguished into persistent activity at the summit craters and periodic flank eruptions. The former is characterized by phases of degassing alternating with mild strombolian activity, occasional lava fountains, and lava overflows. Flank eruptions occur from lateral vents usually located along fracture systems. The past decade at Mt. Etna was characterized by different kinds of activity. From 2001 to 2003, two large eruptions characterized by very intense explosive activity took place in the southern and northeastern flanks of the volcano. Successively, Etna remained quiet for about 20 months up to September 2004 when an eruption, differing significantly from the two previous, erupted essentially degassed magma from two vents within Valle del Bove (e.g. Di Grazia et al., 2006). After a 15-month-long period mainly characterized by degassing, the eruptive activity resumed on the eastern flank of SEC in late 2006 with strombolian activity, lava fountaining and lava overflows. During 2007, six episodes of intense lava fountaining/strombolian activity took place at SEC. Finally, after a lava fountain occurring on 10 May 2008 at SEC, a new eruption took place on 13 May from an eruptive fissure that opened east of the summit area (EF; Cannata et al., 2009c; **Fig. 10**). This eruption, ending on 6 July 2009, was characterized by a strong Hawaiian activity at its beginning and by a long phase of gradually decreasing strombolian activity and lava flows during the following months (Aloisi et al., 2009).

3. Mt. Etna's deep plumbing system: tomographic analysis

Since 1977, seismic surveys and seismological studies have progressively improved our knowledge of Etna's structure, but there is still no clear evidence for the presence of a large magma chamber in the crust. In the last two decades, tomographic inversions of P- and S-wave arrival times from local earthquakes have been performed with various techniques allowing a good definition of the P-wave velocity structure beneath the volcano down to 18-24 km depth, more detailed down to 10 km depth (Chiarabba et al., 2000; Laigle et al., 2000; Patanè et al., 2002; Chiarabba et al., 2004; Patanè et al., 2006). However, none of these studies have evidenced the presence of a large anomalous region of relatively low-velocity in the upper crust beneath the volcano. One of the recent ideas about the deep structure of Mt. Etna is the presence of a melted lens capping a mantle upward beneath the volcano (Hirn et al., 1997) with a Moho transition at less than 20 km deep (Nicolich et al., 2000). Following, the main features revealed by Mt. Etna velocity and attenuation tomographies are reported and discussed.

3.1 Active seismic surveys and tomographic studies

The first noteworthy seismic investigation of the crust and upper mantle in Sicily was performed in 1968 by seismic refraction surveys and covered the whole island with only one profile near Etna, located just to the north (Cassinis et al., 1969). The interpretation of seismic sections revealed a low velocity zone in the eastern Sicily continental crust, close to Mt. Etna between 9 and 24 km depth, interpreted as a region with high temperatures due to the proximity of a deep magma chamber under the volcano. Following this early active seismic exploration, only in 1977 a deep seismic sounding focused on Etna's structure, with both a detailed survey and deployment of a temporary seismic array (Colombi et al., 1979). Based on data acquired during these experiments, Sharp et al. (1980) investigated Mt. Etna's structure and the physical properties of the low-velocity anomaly previously observed near the area. They modelled this anomaly as a low-velocity, tri-axial ellipsoid body extending under the entire volcanic area at midcrustal depths (15-25 km), interpreted as a large partially molten magma chamber.

Since the 90's, seismological studies have progressively improved our knowledge of Etna's structure and in the last two decades, tomographic inversions of P- and S-wave arrival times from local VT earthquakes have been performed with various techniques (Hirn et al., 1991, 1997; Cardaci et al., 1993; De Luca et al., 1997; Laigle et al., 2000; Chiarabba et al., 2000; Patanè et al., 2002; Patanè et al., 2003; Chiarabba et al., 2004). None of these tomographic studies showed the presence of a large anomalous region of relatively low-velocity within the crust beneath the volcano interpretable as a large magma chamber. Conversely, the most important feature is the presence of a wide central high-velocity body (HVB) embedded in the pre-Etnean sediments, interpreted as a main solidified intrusive body (cooled batches of magmatic intrusions), which is also an almost aseismic volume surrounded by an active seismic region. This HVB shows a roughly ellipsoidal shape in the upper crust (depth ~10 km) with a NNW-SSE horizontal axis and a vertical axis extending between 0 and 9 km below sea level. However, basalt melt rising through the continental intermediate crust may not produce a slow anomaly and the clear large high Vp body observed in the tomographic images can be related to the volumes where the magma is stored in the crust before the eruption. This seems to be supported by the existence of the wide, elongated aseismic zone located just beneath the summit craters (Chiarabba et al., 2000; Patanè et al., 2004) and by results regarding the spatial distribution of b-values (Murru et al., 1999). De Gori et al. (2005)

tried to yield insights into the physics of the volcanic plumbing system by determining the three-dimensional Qp structure. This attenuation tomography evidenced the presence of a low Qp body located at shallow depth (0–3 km b.s.l.) beneath the south and southwestern sides of the edifice, where the magma was likely stored during 1994–2001. Since attenuation is a physical parameter sensitive to the thermal state of the crustal volume traveled by seismic wave, this interpretation of the low-Qp anomaly, also confirmed by Martinez-Arevalo et al. (2005) for the 2001 eruption, is consistent with the intense recent volcanic activity (2001 and 2002–2003) that concentrated in the southern part of the summit area. Finally, the Patanè et al. (2006) inversion allowed the improvement of even the most recent velocity tomographic results (Patanè et al., 2002; Patanè et al., 2003; Chiarabba et al., 2004) and a better definition of the shallow structure, down to 7 km depth, and shape and geometry of the upper portion of high-velocity Vp volume. However, the most notable result of this work concerns the detection of anomalous zones with low Vp/Vs values located in the central-southern and northeastern part of the volcanic edifice, where geodetic data modeled the dike intrusions feeding the 2002–2003 eruption, located beneath the eruptive fracture systems.

3.2 Shape and geometry of the intermediate and deep plumbing system

Mt. Etna's tomographic models contribute significantly to clarify whether and how tectonic control of magma ascent works at Mt. Etna, revealing a broad complex of intrusive meshes in the upper and middle crust. In particular, we analyze the results obtained by the last tomographic study performed by Patanè et al. (2006) integrating it with previous results and new unpublished data. In summary, the main features revealed by Mt. Etna Vp tomography (Patanè et al. 2006, **Fig. 3a**) are:

- A shallow high Vp anomaly (Vp ranging between 3.5 and 5.5 km/s) beneath the southern craters, the South Rift and mostly beneath the central-southern sector of the Valle del Bove, between 0 and -1 km depth, is interpreted as a solidified intrusive complex (**Fig. 3a**). Contours for 3.5-5.0 km/s at 0 km show that the high velocity anomaly aligns with the present-day south and northeastern Rifts. The presence of the old shallow plumbing system feeding the past Mt. Etna eruptive centers (e.g. Trifoglietto volcano), located along the central-southern part of the Valle del Bove, is also evidenced both at 0 and -1 km a.s.l.. The analysis of the isosurface image at Vp of 3.5 km/s (**Fig. 3b**), reveals a complex pattern of solidified magma chambers and conduits with variable dimensions in the very shallow crust (between 0 and -1 km a.s.l.). These higher velocity volumes can be linked to: i) the wide plutonic body mainly located beneath the Valle del Bove (Patanè et al., 2003, 2006); ii) the solidified magma reservoirs feeding the S, NE and ENE Rift zones.
- A clear high Vp body (Vp ranging between 5.5 and 6.7 km/s), NNW-SSE to NS trending located beneath the central craters extended toward S and SSE, between -2 and -7 km a.s.l. (wide 5-7 km in longitude and 8-10 km in latitude) is interpreted as high density cumulates, fractionated by the magma during its ascent, stocked and congealed at depth (**Fig. 3 a**).

Considering now the two different inversions by Patanè et al. (2003) and Chiarabba et al. (2004), extended also to the deep structure although at lower resolution, the main features observed at major depth are:

- A narrow high Vp body (Vp ranging between 6.8 and 7.5 km/s), 4-6 km laterally wide, beneath the central-southern part of the volcano between 8 and at least 18 km depth (**Fig. 4a**), interpreted as the deeper part of the plumbing system.

- The presence of a melted lens capping a mantle upward beneath the volcano with a Moho transition at depth less than 20 km (**Fig. 4a, b**), as suggested by Nicolich et al. (2000), seems to be supported by recent tomographic results at regional scale (Barberi et al., 2006).

Therefore the high Vp intrusion is the main structural feature of the volcano, testifying to its intense past history, and revealing the accumulation of a very large volume of non-erupted volcanic material. Seismicity seems to occur at its borders and defines a main aseismic volume (**Fig. 3b**).

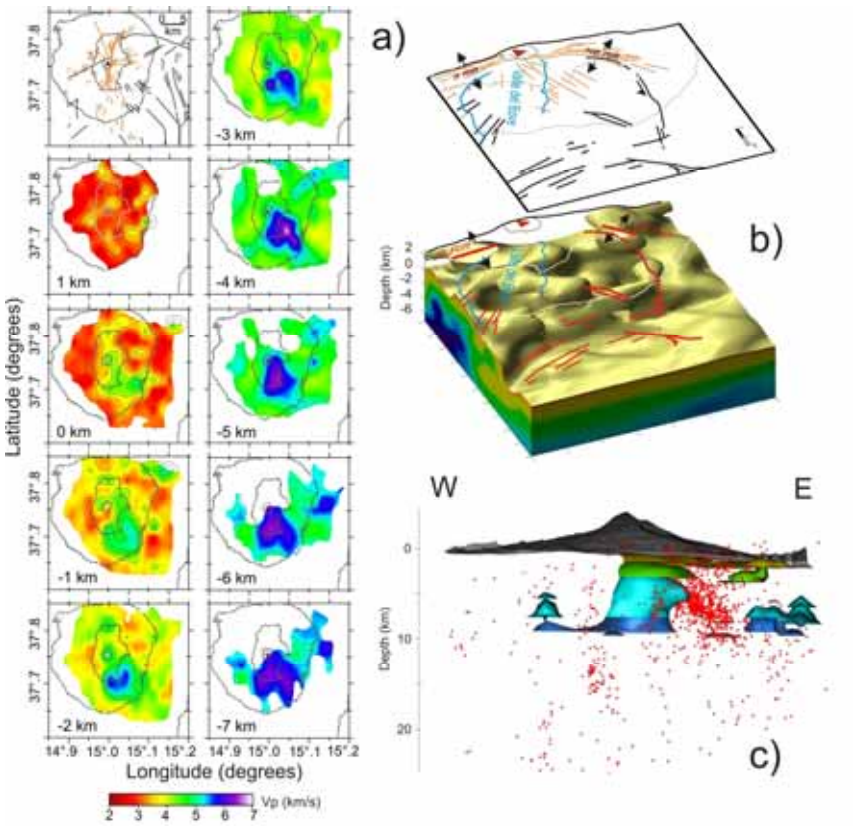

Fig. 3. (a) Mt. Etna's Vp velocity model (Patanè et al. 2006), between 1 a.s.l. and 7 km b.s.l., in the well-resolved regions of the model . The gray lines are elevation isolines (every 1000 m). In the top left square the historical eruptive fissures (orange lines) and major faults (black lines) are shown. b) Isosurface image at Vp of 3.5 km/s for the central-eastern and northern sectors of the volcano. A complex pattern of solidified magma chambers and conduits with variable dimensions is recognizable. At the top, historical eruptive fissures (orange lines) and major faults (black lines) are shown. Major faults are also projected in red in the 3D block. c) Cumulative isosurfaces for different velocities Vp showing the 3D geometry of the HVB down to 10 km depth. The seismicity occurring during 2001-2003 is also shown (red dots), evidencing how the HVB is almost an aseismic volume surrounded by an active seismic region

The bulk of the high Vp body, located to the southeast of the central craters, suggests that the Valle del Bove has been the main site for magma accumulation in the past as confirmed by the presence of the old eruptive centers (e.g. Trifoglietto). The high Vp body NNW-SSE to NS trending between -1 and -5 km depth appear rooted at greater depth. At present, the ascent of magma is controlled by the pervasive high Vp intrusion and seems to occur at its western border. Very shallow dike emplacement at the border of the intrusive body occurs mostly on NNW-trending fracture system, such as those of the 2001 and 2002-2003 eruptions.

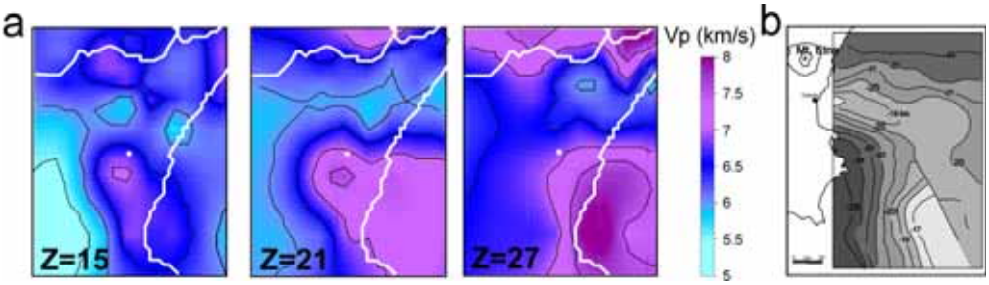

Fig. 4. a) Regional Vp model of the lower crust and uppermost mantle from Barberi et al. (2006). b) Moho topography (km b.s.l) of the northwestern part of the Ionian basin (redrawn from Nicolich et al., 2000)

4. Mt. Etna shallow plumbing system: seismo-volcanic signal analysis

Although the VT earthquakes are the key to tomographic studies in volcanoes, they cannot provide precise information about the location and geometry of the shallow magma conduits (Almendros et al., 2002). In fact, the understanding of the complex velocity structure in the shallow part of the volcano requires estimation of both P- and S- waves variations with a spatial resolution of the order of several hundred meters, which is still not yet available at Mt. Etna.

A more useful approach consists of investigating the seismo-volcanic signals, whose variations and features are often closely related to eruptive activity. Indeed, they are generally considered as an indicator of the internal state of activity of volcanoes (Neuberg, 2000). For this reason their investigation can be very useful for both monitoring and research purposes. Because of the peculiar characteristics of the seismo-volcanic signals, different from the tectonic and VT earthquakes in terms of both waveforms and source mechanisms, new techniques have been developed to investigate their features. In **Fig. 5** examples of VT earthquake, volcanic tremor, LP and VLP events recorded at Mt. Etna are shown.

According to Murray (1990), shallow reservoirs at Mt. Etna are temporary and are occupied by magma only during short periods preceding a single eruption or an eruptive cycle. Patanè et al. (2008) demonstrated how the locations of the tremor sources and of the long-period seismic events can be used at Mt. Etna to constrain both the area and the depth range of magma degassing, highlighting the geometry of the shallow conduits feeding the central craters. In this work the Authors, by a careful analysis of the seismo-

volcanic signals recorded during two powerful lava fountaining episodes taking place on 4–5 September and on 23–24 November, 2007 from SEC, discover the magma pathway geometry feeding the eruptive activity at SEC. The imaged conduits consist of two connected resonating dike-like bodies, NNW-SSE and NW–SE oriented, extending from sea level to the surface. In addition, we show how tremor, long-period (LP), and very-long period (VLP) event locations and signatures reflect pressure fluctuations in the plumbing system associated with the ascent/discharge of gas-rich magma linked to the lava fountains.

Thus, in this section we will focus on the most recent eruptive activity of this volcano taking place in 2008-2009, showing the inferences about the volcano dynamics and the shallow system feeding this eruption drawn by the seismo-volcanic signal investigation. **Fig. 6** shows a digital elevation model of Mt. Etna with the locations of the stations used to record the seismic signals during such an eruption. In **Fig. 7** the seismic signal acquired by the vertical component of ECPN during 1-13 May 2008, together with the number of LP events and the seismic RMS, is shown.

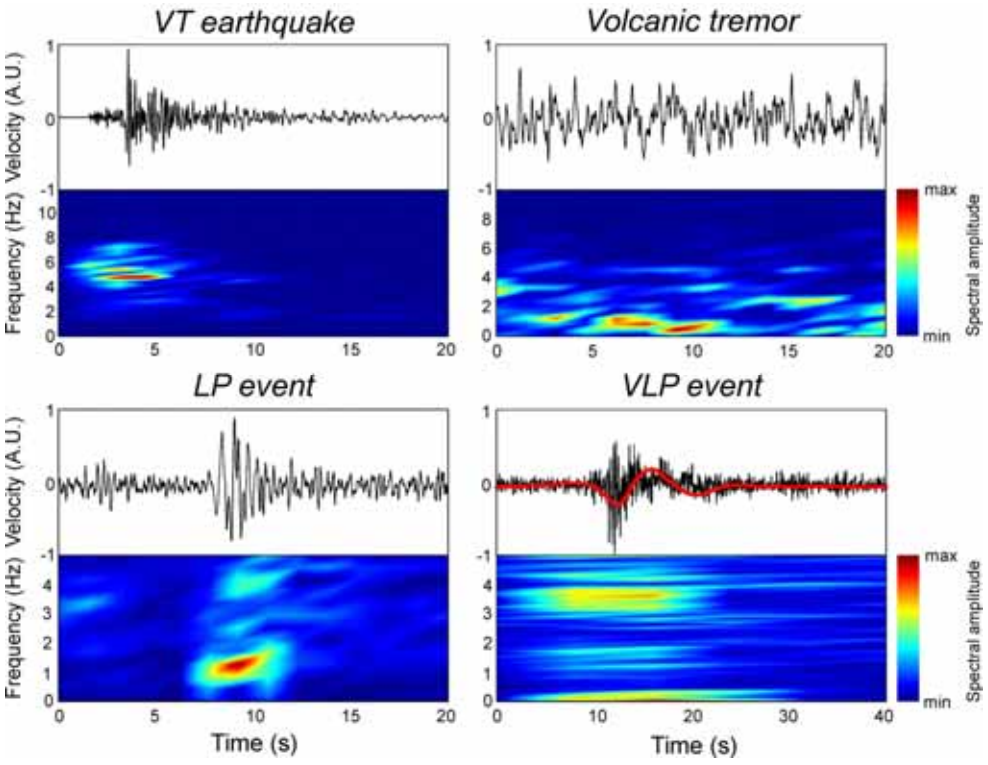

Fig. 5. Waveforms and spectrograms of VT earthquake, volcanic tremor, LP event and VLP events recorded at Mt. Etna. The thick red line plotted over the VLP waveform shows the signal filtered below 0.15 Hz

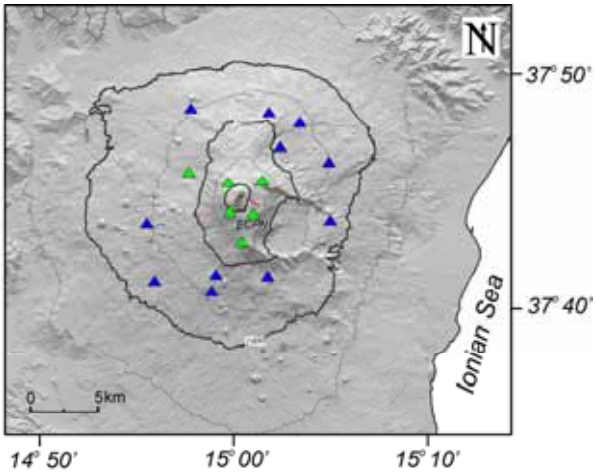

Fig. 6. Digital elevation model of Mt. Etna with the location of the seismic stations used to investigate seismo-volcanic signals (green and blue triangles). The green triangles indicate the stations used to study both volcanic tremor and LP events, while the blue triangles only the volcanic tremor. The red line indicate the eruptive fissure active during 2008-2009

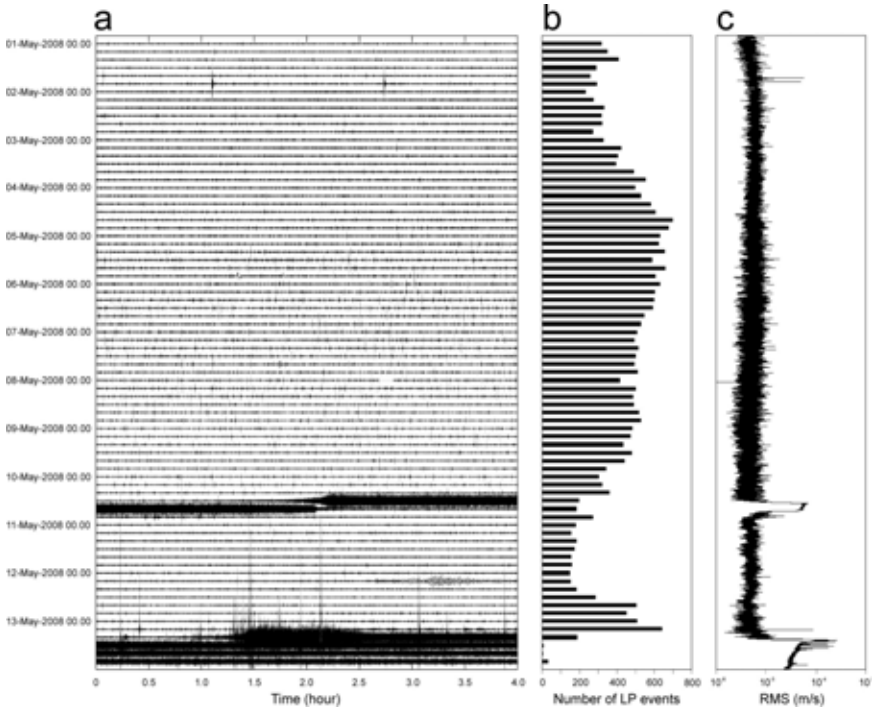

Fig. 7. (a) Seismogram of the vertical component of ECPN station, (b) histogram of the number of LP events in 4-hour-long windows and (c) RMS time series

4.1 Volcanic tremor and LP events

A peculiar aspect of volcanic tremor at Mt. Etna is its continuity in time, as also observed at other basaltic volcanoes with persistent activity such as Stromboli (Italy; Langer and Falsaperla, 1996). Most of the energy of volcanic tremor at Mt. Etna is radiated below 5 Hz (e.g., Lombardo et al., 1996; Falsaperla et al., 2005; Cannata et al., 2008, 2009a). Another interesting feature of the volcanic tremor is its close relationship to eruptive activity, highlighted by variations in amplitude, spectral content, wavefield features, and source

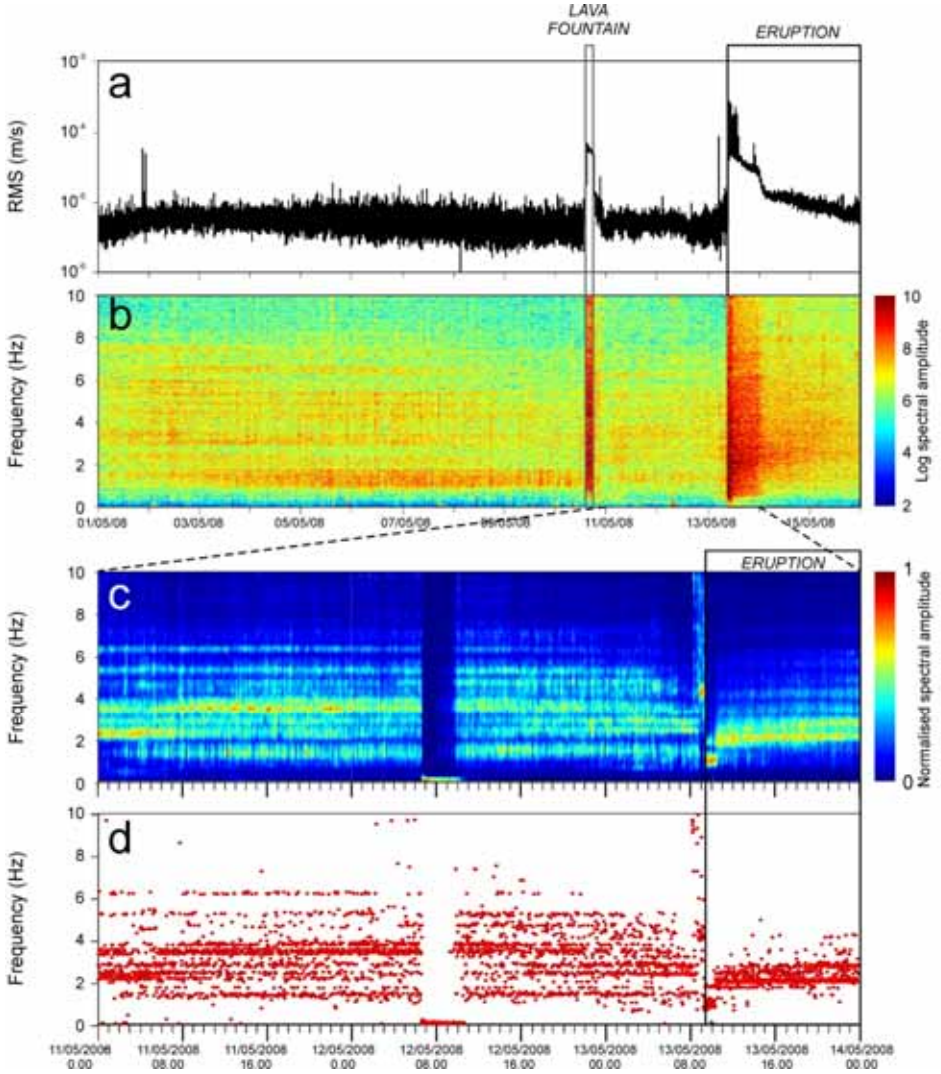

Fig. 8. (a) RMS time series and (b) spectrogram of the seismic signal recorded at the vertical component of ECPN station. (c) Normalised spectrogram and (d) dominant frequencies of the seismic signal recorded at the vertical component of ECPN station

location of volcanic tremor at the same time as changes in volcanic activity (e.g., Gresta et al., 1991; Lombardo et al., 1996; Di Grazia et al., 2006; Alparone et al., 2007; Cannata et al., 2008; Patanè et al., 2008; Cannata et al., 2009a). The volcanic tremor recorded during 1–15 May 2008 was investigated by performing several analyses. First of all, in order to get information about the time changes of tremor energy, the RMS of the seismic signals recorded at the vertical component of ECPN station (see **Fig. 6**) was calculated within 1-minute-long sliding windows (**Fig. 8a**). Successively, since changes of source location and/or mechanism of volcanic tremor are generally accompanied by variations of its spectral content, the Short Time Fourier Transform (STFT) was performed. We calculated a spectrum by 40-secong-long sliding windows of the signal recorded at the vertical component of ECPN station. Then, the spectrogram was plotted in **Fig. 8b**. Moreover, the normalized spectrogram of 11-14 May, together with the dominant frequencies, was also computed and plotted in **Fig. 9c,d**. Finally, since the seismo-volcanic signals are generally related to dynamics of fluid inside the volcanic edifice, the location of their source is basic information for monitoring of volcanoes. Then, the tremor source locations were retrieved by following the approach described by Patanè et al. (2008) and Di Grazia et al. (2009), inverting the spatial distribution of tremor amplitude in 18 stations (green and blue triangles in **Fig. 6**) using a grid-search approach (**Figs. 9,10**). We considered the RMS amplitudes of the 25th percentile instead of average values. This enables us to efficiently remove undesired transients in the signal and consider continuous recordings (Patanè et al., 2008). The source location of tremor is found on the basis of the goodness of the linear regression fit (hereafter referred to as R^2) obtained for each point of a 3-D grid centered underneath the craters (Di Grazia et al., 2006). For this grid, we consider a $6 \times 6 \times 6$ km^3 volume with a spacing between nodes of 250 m. The centroid position of all the 3-D grid points, whose R^2 values do not differ by more than 1% from the maximum R^2, was considered the tremor source location. LP and VLP events, whose sources, similar to volcanic tremor, are related to fluid processes (such as vibration or resonance of fluid-filled cracks; Chouet, 2003), are also recorded at Mt. Etna. A number of papers deal with the relation between eruptive activity and LP events at Mt. Etna (Patanè et al., 2008; Di Grazia et al., 2009; Cannata et al., 2010): it was shown how occurrence rate, energy, spectral content and/or source location of LP events often change before, during and after eruptive activities. LP events recorded during 1 – 15 May 2008 were investigated obtaining several parameters: i) occurrence rate; ii) peak-to-peak amplitude; iii) source location. About 33,000 LP events were detected during the analysed period by STA/LTA algorithm (short time average/long time average; e.g., Withers et al., 1998). Similar to all the triggering algorithms based on dynamic thresholds, the event detection by STA/LTA is affected by the variation of the background noise level: for instance, if the background noise level increases, the threshold in turn will increase, and then the events with lower amplitude will be lost. The LP hourly number and the peak-to-peak amplitudes were calculated and plotted in **Fig. 11a,b**, respectively. Moreover, since the frequency and damping of a resonant system is strongly influenced by the nature of liquid and gas content (Chouet, 2003 and references therein), also the study of the spectral evolution of LP events in volcanic areas provides very useful information for monitoring purposes. Thus, a value of frequency and quality factor for each LP event were obtained by Sompi analysis (Kumazawa et al., 1990) (**Fig. 11c,d**). A moving median over 200 samples was calculated for both frequency and quality factor. Indeed, the median values are less affected by outliers than the average values. Finally, a subset of 1700 LP events with high signal to noise ratio at all the six stations nearest to the summit area (green triangles in **Fig. 6**) was selected to perform

location analysis. LP events were located by following a new grid-search method based on the joint computation of two different functions: i) semblance, used to measure the similarity among signals recorded by two or more stations (e.g. Neidell and Taner, 1971; Cannata et al., 2009b); and R^2 values, calculated on the basis of the spatial distribution of seismic amplitude (Patanè et al., 2008; Di Grazia et al., 2009). The 3-D grid of possible locations was 6 km×6 km×3.25 km, centered on the volcanic edifice, and with a vertical extent from 0 km a.s.l. to the top of the volcano. The horizontal and vertical grid spacing was 250 m. The space distributions of both semblance and R^2 values were determined, the two grids of values were normalised by subtracting the minimum value and dividing by the maximum one. Thus, the values belonging to two grids ranged from 0 to 1, and the same weights were assigned to semblance and R^2. Then, the two normalised grids were summed node by node. The source was finally located in the node with the largest composite semblance-R^2 value. This joint method takes advantage of both LP waveform comparison among the different stations and space amplitude distribution. The LP location results are reported in **Figs. 12** and **13**.

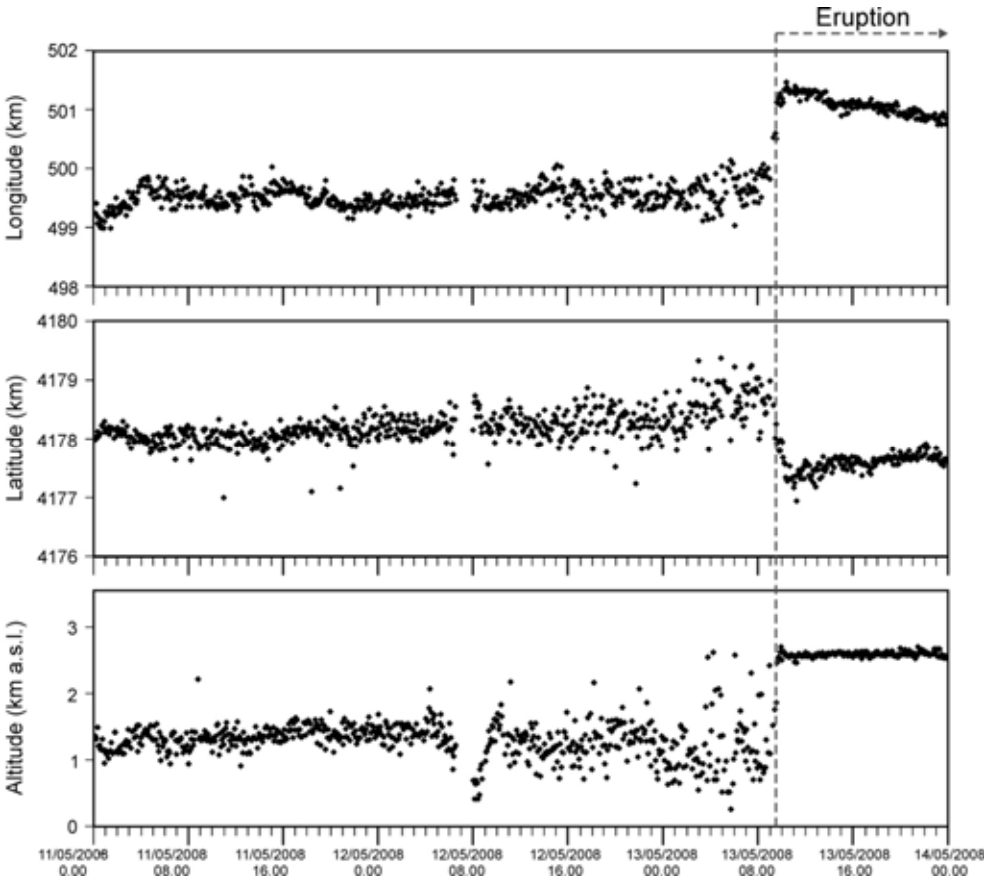

Fig. 9. Time variations of the location of volcanic tremor recorded during 11-14 May 2008

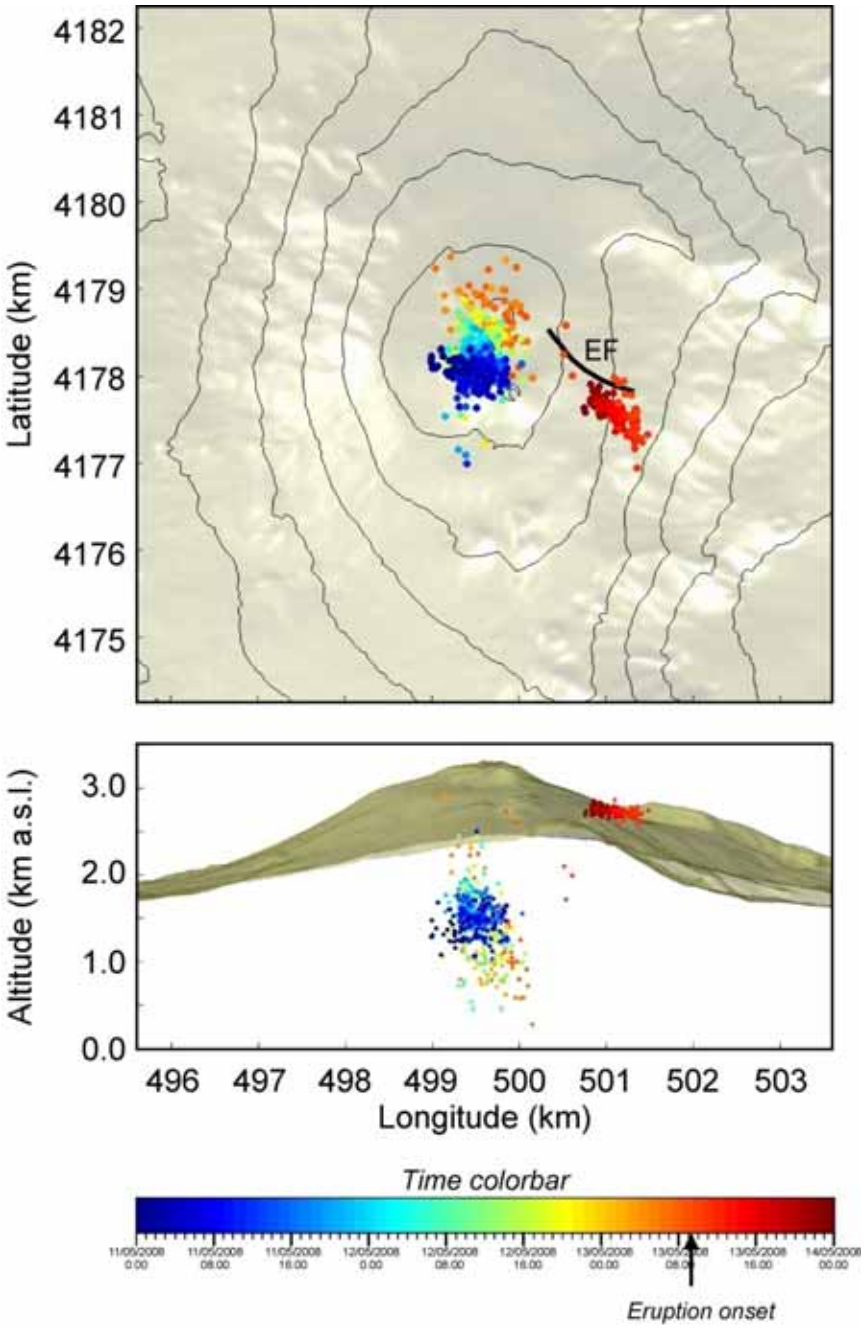

Fig. 10. Map and section of Mt. Etna with the locations of volcanic tremor recorded during 11-14 May 2008

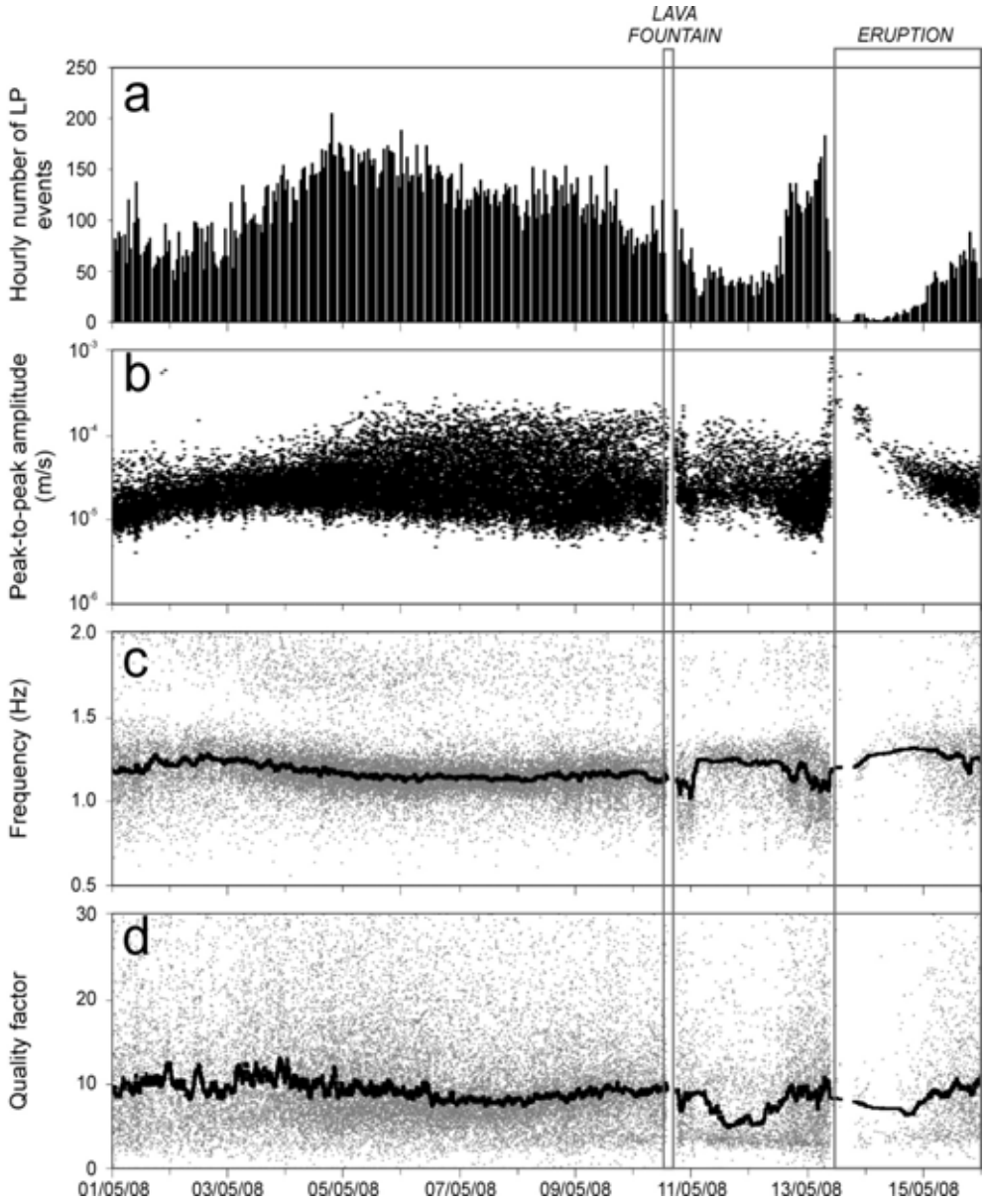

Fig. 11. (a) Histogram of the number of LP events in 1-hour-long windows. (b) Peak-to-peak amplitude of the LP events. (c,d) Frequency and quality factor of the LP events, calculated by Sompi method with autoregressive order of 2

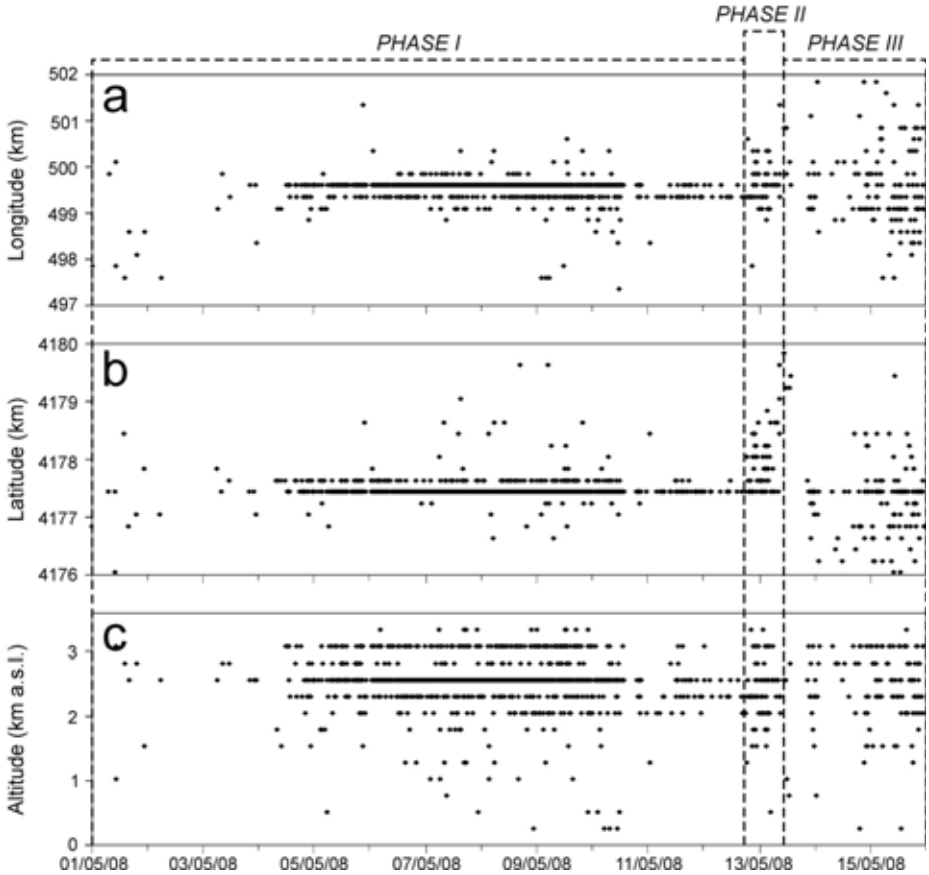

Fig. 12. Time variations of the location of LP events recorded during 1-15 May 2008

Finally, in order to understand the LP source mechanisms, moment tensor inversions were performed. On several volcanoes Moment Tensor Inversion has been achieved to quantify the source processes of LP events (e.g. Ohminato et al., 1998; Chouet et al., 2003; Lokmer et al., 2007). Indeed, due to the link between LP activity and fluid dynamics (Chouet, 2003), the characterization of the LP source mechanism becomes a fundamental tool for understanding processes in magmatic systems. Several studies propose the excitation and resonance of fluid-filled resonator systems as the cause of the source mechanism of these particular events. Different geometries of the resonators were investigated, such as a crack, a spherical inclusion or a conduit simplified to a cylinder. The seismic moment-tensor is a representation of a seismic source by a system of equivalent forces acting at a source point, including the force couples and single forces resulting from mass transport. We performed a moment tensor inversion in the frequency domain (Auger et al., 2006; Lokmer et al., 2007). The Green's Functions (GF) are calculated for a homogeneous velocity model with DEM Etna topography. Synthetic seismograms were generated by Discrete Elastic Lattice algorithm described by O'Brien and Bean (2004), based on discrete particle scheme. The topography model of Mt. Etna covers an area of 19.2 x 16 x 7 km, with a grid node of 50 m,

and its origin (x,y,z) is centred on the volcano summit. In order to avoid reflections from the model boundaries, we employed at the bottom and at the edges of the model 4.8 km wide absorbing boundaries. Moreover we used for the GF computation (i) a Gaussian pulse as source function (STF), with a 7.5 Hz cut-off frequency; (ii) velocities for P and S waves of 2000 ms^{-1} and 1175 ms^{-1} respectively, as found by Patanè et al. (2006) and Montellier et al. (2009) in their recent tomographic study of Mt. Etna. Several authors demonstrated how the topography and the velocity model play an important role to correctly reconstruct the moment tensor (e.g. Bean et al., 2008; O'Brien and Bean, 2009). For LP events, which are characterized by frequencies above 5 seconds, uncertainties in the GF can be introduced by a poor knowledge of the velocity structures. This problem can be resolved by using several seismic stations installed very close to the source positions (Bean et al., 2008; Kumagai et al., 2010; De Barros et al., 2011). For this reason, in order to compute the LP moment tensor inversion, we used the LP database recorded by an exceptionally high-density network of 30 temporary broadband stations, installed during the 2008-2009 Etna eruption (De Barros et al., 2011). In order to determine the most reliable mechanism type (crack, pipe, or explosion), the source of the LP is initially modelled performing an unconstrained inversion. Next, starting from the mechanism so obtained, we have constrained the subsequent reversals solution (inversions) found to confirm and refine its characteristics. Once the stability of our results is verified, it was possible to reconstruct the source mechanisms of the LP in 2008 Etna eruption.

4.2 Results and interpretation

The analyses described in the **section 4.1** provided information about the volcano dynamics and on the shallow part of the plumbing system involved in magma movements before and during the first days of the eruption.

The 10 May lava fountain and the following 13 May eruption onset were preceded by a change in the volcanic tremor spectral content (from polychromatic to monochromatic with a spectral peak at 1-2 Hz) and by an increase in LP activity (increases in both occurrence rate and amplitude of LP events) taking place roughly on 4 May. Such an energy increase of LP events can be interpreted as increasing overpressure inside the shallow part of the plumbing system. Increases of amplitude and occurrence rate of LP events preceded eruptive activities also at many other volcanoes such as Redoubt (Chouet et al., 1994), St. Helens (Moran et al., 2008) and Colima (Varley et al., 2010). Before the eruptive activity the volcanic tremor was located below the summit area at depth ranging from 1 to 2 km a.s.l. (**Figs. 9,10**), suggesting an important magma storage volume in this location, as also suggested by previous studies (Allard et al., 2005; Aiuppa et al., 2010). The LP events were located roughly below Bocca Nuova at 2-3 km a.s.l., consistent with the LP location obtained in other papers (Patanè et al., 2008; Cannata et al., 2009b). The lava fountain was accompanied by a sharp increase in the tremor RMS, as observed during other lava fountain activities at Mt. Etna (e.g. Cannata et al., 2008), as well as at other volcanoes (e.g. McNutt, 1994). Because of this increase of tremor amplitude and then of the background noise level, only a few LP events were detected during the lava fountain (**Fig. 11a**). It is also worth noting that during the whole of 10 May the LP frequency peak decreased, then suddenly increasing on the following day (**Fig. 11c**). After the lava fountain, the sudden decrease in the seismic dominant frequencies observed during 06.00-11.00 on 12 May was due to the arrival of teleseismic waves of the Sichuan earthquake (M=7.9) that, according to Cannata et al. (2010), played an important role in the 13 May eruption because of the dynamic stress transfer. Focusing on the 13 May eruption, it was preceded by a few hours by a further increase in the LP activity,

accompanied by changes in LP spectral content (decrease of frequency peak and increase of quality factor; **Fig. 11c,d**), and by a northward shift of the sources of both volcanic tremor and LP events (**Figs. 10,13**). Such a seismo-volcanic source migration was consistent with the dyke intrusion in the northern part of the summit area (towards the NE rift zone; **Fig. 2**), inferred by earthquake swarm hypocenters (Di Grazia et al., 2009), ground deformation (Aloisi et al., 2009) and a dry fracture field (Bonaccorso et al., 2011). Finally, the onset of the 13 May eruption was characterised by a sharp RMS increase reaching the maximum values of the whole analysed period (**Fig. 8a**), together with significant changes in spectral content (**Figs. 8c,11**) and shift of tremor and LP sources moving roughly below the eruptive fissure (**Figs. 9,10,12,13**). Also in this case the LP number drastically decreased because of the increase of the background noise level (**Fig. 11a**). All these data suggest the intrusion of a gas-rich magma batch east of the summit area.

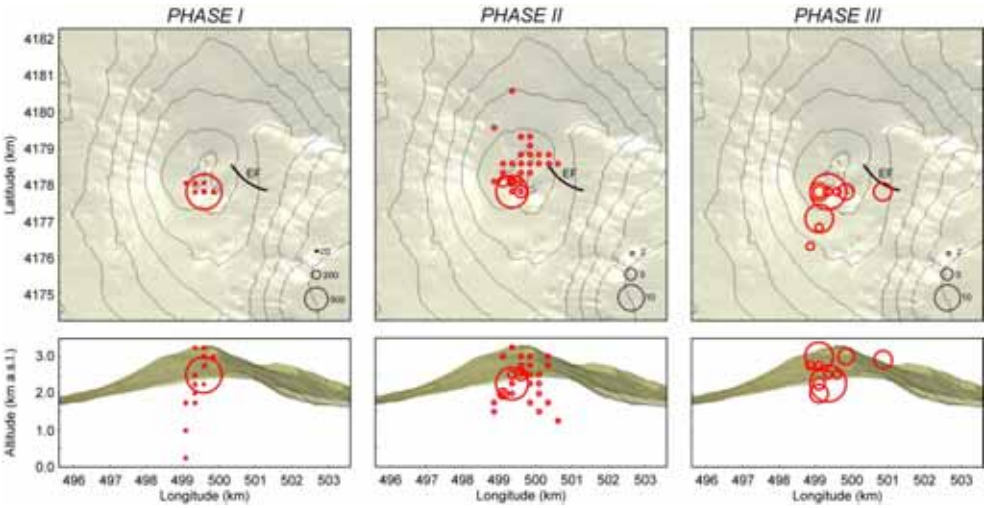

Fig. 13. Map and section of Mt. Etna with the locations of LP events recorded during three phases (see dashed black lines and "phase I", "phase II" and "phase III" in Fig. 12). The radii of the red circles are proportional to the number of the locations in each grid node (see black circles and numbers reported in the right lower corner of the maps)

Between 18 June and 3 July 2008, about 30 temporary broadband stations were deployed on Mt. Etna very close to the summit craters. This high-density network permitted to better investigate on the LP activity. De Barros et al. (2009), classifying more than 500 LP events by cross-correlation analysis, obtained two different families with a similar number of events. In agreement with previous studies (e.g. Saccorotti et al., 2007; Cannata et al., 2009b), the LP source positions were located close to the summit craters, and were slightly different for both families. The focal depth hypocentres were found shallow below the summit: from 0 to 800 m for family 1 and from 0 to 400 m for family 2 (De Barros et al., 2009). For both families the inversions show mechanisms with high volumetric components, most likely generated by a crack, striking in the SW-NE direction (De Barros et al., 2011). In particular for family 1 (**Fig. 14a**) the MT solution shows a subvertical dike striking SSW-NNE; for family 2 the crack solution lies on a plane inclined of 45° and striking SW-NE (**Fig. 14b**). The orientations

of the cracks are consistent with local tectonics, which shows a SW–NE weakness direction, as testified by the orientation of the NE rift. De Barros et al. (2011) hypothesize that these events are not related to the lava flow from the eruptive fracture, instead to the decompression phase following the 10 May lava fountain. The LP events studied here show similar characteristics to the events occurring after a lava fountain in the 2007, analysed by Patanè et al. (2008), which interpreted, in particular, the LP belonging to the family 2 as the response to the volcano deflation. This theory is validated by the temporary cessation of the LP events after 22 June 2008, suggesting a return of equilibrium of the upper part of volcano, where pressure and stress return to a static state. Although the poor knowledge of the velocity model can lead to unambiguous explanations of both moment and forces related to the mechanism found, this study demonstrated how the LP moment tensor inversion is a powerful tool to understand the magmatic processes in the shallow plumbing system of Mt. Etna.

In summary, it was shown how the analysis of seismo-volcanic signals is very effective to reconstruct the geometry of the shallow portion of the plumbing system and to investigate the magma dynamics in it. Such information is very important for both research and monitoring purposes.

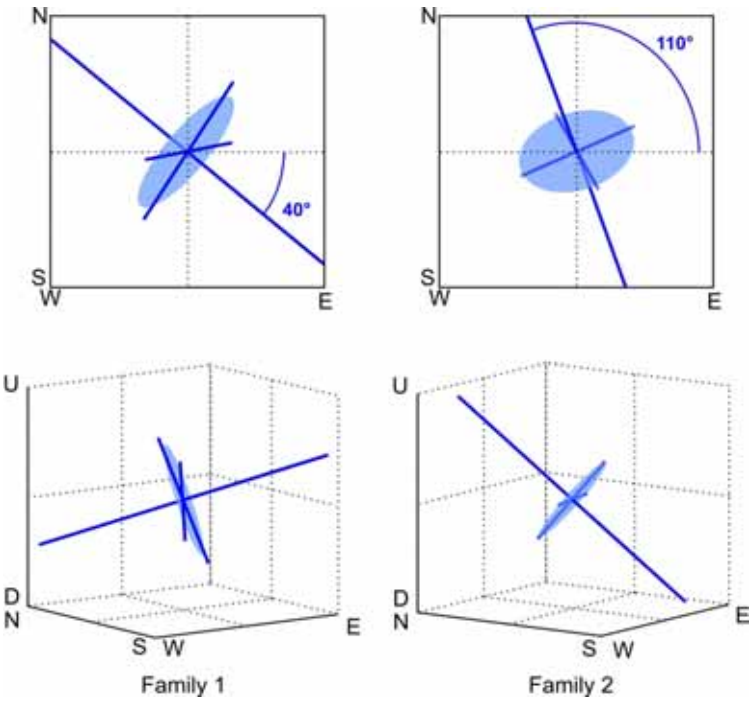

Fig. 14. Map views (up) and 3-D views (down) of the crack source mechanism obtained for the two families of LP events. The circular areas represent the cracks, the normalized eigenvectors are represented by solid lines, and the longest of these are the normal cracks. A subvertical dike striking SSW-NNE is obtained for family 1, and a crack striking SW-NE that lies on a plane inclined of 45° is computed for family 2. Redrawn from De Barros et al. (2011)

5. Summary

Mt. Etna lies in front of the southeast-verging Apennine-Maghrebian fold-and-thrust belt, where the NNW-trending Malta Escarpment separates the Sicilian continental crust from the Ionian Mesozoic oceanic basin, presently subducting beneath the Calabrian arc (Selvaggi and Chiarabba, 1995). Seismic tomographic studies indicate the presence of a mantle plume beneath the volcano with a Moho transition at depth less than 20 km (Nicolich et al.,2000; Barberi et al., 2006). Geophysical and geological evidences suggest that the Mt. Etna magma ascent mechanism is related to the major NNW-trending lithospheric fault (Doglioni et al., 2001). However, the reason for the Mt. Etna mantle plume draining and channeling the magma from the upper mantle source to the surface is not yet clear. All models proposed in literature (Rittmann, 1973; Tanguy et al., 1997; Monaco et al.; 1997; Gvirtzman and Nur, 1999; Doglioni et al., 2001) do not explain why such a mantle plume has originated in this anomalous external position with respect to the arc magmatism and back-arc spreading zones associated with the Apennines subduction. Some ideas on the subduction rollback must be better developed through the comparison with new regional tomographic studies that are being released. Moreover, tomographic studies reveal a complex and large plumbing system below the volcano from -2 to -7 km a.s.l., wide up to 60 km² that reduces itself in size down to -18 km of depth close to the apex of the mantle plume. Chiocci et al. (2011) found a large bulge on the underwater continental margin facing Mt. Etna, and suggested that the huge crystallized magma body intruded in the middle and upper continental crust was able to trigger an instability process involving the Sicilian continental margin during the last 0.1 Ma. This phenomenon induces the sliding of the volcano eastern flank observed since the 90s (Borgia et al, 1992; Lo Giudice and Rasà, 1992) because the effects of the bulge collapse are propagating upslope, and the continuous decompression at the volcano summit favors the ascent of basic magma without lengthy storage in the upper crust, as one might expect in a compressive tectonic regime. Taken together, these new evidences (tomographic, tectonic, volcanic) are concerned with the exceptional nature of Mt. Etna and raise the need to explain the origin of the mantle plume that supplies its volcanism. The lower crust and the uppermost mantle need to be better resolved in future experiments and studies. The use of regional and teleseismic events for tomography and receiver function analyses is required to explore a volume that has only marginally been investigated to date. The relation between the magma source in the mantle and the upper parts of the system, as well as the hypothesis above reported on the relation between tectonics and volcanism and the role of lithospheric faults, could be resolved only by applying seismological techniques able to better constrain broader and deeper models.

Finally, although the recent tomographic inversions have progressively improved our knowledge of Etna's shallow structure, highlighting a complex pattern of magma chambers and conduits with variable dimensions, the geometry of the conduits and the dimensions and shapes of small magmatic bodies still require greater investigation. Their precise definition is crucial to delineate a working model of this volcano in order to understand its behaviour and evolution. For this purpose, at least within the volcanic edifice, the precise locations of the seismo-volcanic signals can be considered a useful tool to constrain both the area and the depth range of magma degassing and the geometry of the shallow conduits. In this work, we furnish evidences that the tremor and LP locations allowed to track magma migration during the initial phase of the 2008-2009 eruption and in particular the initial northward dike intrusion, also confirmed by other geophysical, structural and

volcanological observations (Aloisi et al., 2009; Bonaccorso et al., 2011), and the following fissure opening east of the summit area at the base of SEC. All these evidences, obtained by the marked improvement in the monitoring system together with the development of new processing techniques, allowed us to constrain both the area and the depth range of magma degassing, highlighting the geometry of the magmatic system feeding the 2008-2009 eruption.

6. References

Achauer, U., Evans, J.R., & Stauber, D.A. (1988). High-resolution seismic tomography of compressional wave velocity structure at Newberry volcano, Oregon Cascade range. *J. Geophys. Res.*, 93, pp. 10135–10147.

Acocella, V., & Neri, M. (2005). Structural features of an active strike-slip fault on the sliding flank of Mt. Etna. *J. Struct. Geol.*, 27, pp. 343-355.

Acocella, V., Neri, M., & Sulpizio, R. (2009). Dike propagation within active central volcanic edifices: constraints from Somma-Vesuvius, Etna and analogue models. *Bull. Volcanol.*, 71, 219–223.

Aiuppa, A., Cannata, A. , Cannavò, F., Di Grazia, G., Ferrari, F., Giudice, G., Gurrieri, S., Liuzzo, M., Mattia, M., Montalto, P., Patanè, D., & Puglisi, G. (2010). Patterns in the recent 2007-2008 activity of Mount Etna volcano investigated by integrated geophysical and geochemical observations. *Geoch., Geophys., Geosys.*, 11, doi:10.1029/2010GC003168.

Allard, P., Burton, M., & Murè, F. (2005). Spectroscopic evidence for lava fountain driven by previously accumulated magmatic gas. *Nature*, 433, pp. 407-409.

Almendros, J., Chouet, B., Dawson, P., & Bond, T. (2002). Identifying elements of the plumbing system beneath Kilauea Volcano, Hawaii, from the source locations of very-long period signals. *Geophys. J. Int.*, 148, pp. 303–312.

Aloisi, M., Bonaccorso, A., Cannavò, F., Gambino, S., Mattia, M., Puglisi, G., & Boschi, E. (2009). A new dyke intrusion style for the Mount Etna May 2008 eruption modelled through continuous tilt and GPS data. *Terra Nova*, 21, pp. 316–321.

Alparone, S., Cannata, A., & Gresta, S. (2007). Time variation of spectral and wavefield features of volcanic tremor at Mt. Etna (January–June 1999). *J. Volcanol. Geotherm. Res.*, doi:10.1016/j.jvolgeores.2006.12.012.

Auger, E., D'Auria, L., Martini, M., Chouet, B.A., & Dawson, P. (2006). Real-time monitoring and massive inversion of source parameters of very long period seismic signals: An application to Stromboli Volcano, Italy. *Geophys. Res. Lett.*, 33(4), L04301, doi:10.1029/2005GL024703.

Azzaro, R., Branca, S., Giammanco, S., Gurrieri, S., Rasà, R., & Valenza, M. (1998). New evidence for the form and extent of the Pernicana Fault System (Mt. Etna) from structural and soil-gas surveying. *J. Volcanol. Geotherm. Res.*, 84, pp. 143–152.

Azzaro, R. (1999). Earthquake surface faulting at Mount Etna volcano (Sicily) and implications for active tectonics. *J. Geodyn.*, 28, pp. 193-213.

Azzaro, R., Barbano, M.S., Antichi, B., & Rigano, R. (2000). Macroseismic catalogue of Mt. Etna earthquakes from 1832 to 1998. *Acta Vulcanol.*, 12, pp. 3–36.

Azzaro, R., 2004. Seismicity and active tectonics in the Etna region: constraints for a seismotectonic model. In: Bonaccorso, A., Calvari, S., Coltelli, M., Del Negro, C.,

Falsaperla, S. (Eds.), Mt. Etna: Volcano Laboratory. *AGU Geophys. Monogr*., vol. 143, pp. 205–220.

Azzaro, R., Branca, S., Gwinner, K., & Coltelli, M. The volcano-tectonic map of Etna volcano, 1:100.000 scale: morphotectonic analysis from high-resolution DEM integrated with geologic, active faulting and seismotectonic data. In press in *Journal of Geosciences*.

Barberi, G., Patanè, D., Scarfì, L., & Zhang, H. (2006) Tomographic images of Northeastern Sicily and Southern Calabria crust by using TomoDD algorithm, General Assembly of the European Geosciences Union 2006, EGU06-A-04278; SM1-1WE5P-0434

Bean, C., Lokmer, I., & O'Brien, G. (2008). Influence of near-surface volcanic structure on long-period seismic signals and on moment tensor inversions: Simulated examples from Mount Etna. *J. Geophys. Res.*, 113, B08308, doi:10.1029/2007JB005468.

Bellotti, F., Branca, S., & Groppelli, G. (2010). Geological map of Mount Etna West Rift (Italy). *J. Maps*, pp. 96–122, doi:10.4113/jom.2010.1115.

Bonaccorso, A., Bonforte, A., Del Negro, C., Di Grazia, G., Ganci, G., Neri, M., Vicari, A., & Boschi, E. (2011). The initial phases of the 2008-2009 Mt. Etna eruption: a multi-disciplinary approach for hazard assessment. *J. Geophys. Res.*, doi:10.1029/2010JB007906.

Bonforte, A., Guglielmino, F., Coltelli, M., Ferretti, A., & Puglisi, G., (2011). Structural assessment of Mt. Etna volcano from Permanent Scatterers analysis. *Geochemistry*, *Geophysics*, *Geosystems*, 12, doi:10.1029/2010GC003213.

Borgia, A., Ferrari, L., & Pasquarè, G. (1992). Importance of gravitational spreading in the tectonic and volcanic evolution of Mount Etna. *Nature*, 357, pp. 231– 235.

Bousquet, J.C., & Lanzafame, G. (2001). Nouvelle interprètation des fracture des éruption latérales de l'Etna: conséquences pour son cadre tectonique. *Bull. Soc. Geol. Fr.*, 172, pp. 455– 467.

Bousquet, J.C., & Lanzafame, G. (2004) The tectonics and geodynamics of Mt. Etna: synthesis and interpretation of geological and geophysical data. In: *Mt. Etna: Volcano Laboratory*, Bonaccorso, A., Calvari, S., Coltelli, M., Del Negro, C., Falsaperla, S., pp. 29-47, American Geophysical Union, Geophysical Monograph 143.

Branca, S., Carbone, D., & Greco, F. (2003). Intrusive mechanism of the 2002 NE-Rift eruption at Mt. Etna (Italy) inferred through continuous microgravity data and volcanological evidences. *Geophys. Res. Lett.*, 30, doi:10.1029/2003GL018250.

Branca, S., Coltelli, M., & Groppelli, G. (2004). Geological evolution of Etna volcano. In: *Mt. Etna: Volcano Laboratory*, Bonaccorso, A., Calvari, S., Coltelli, M., Del Negro, C., Falsaperla, S., pp. 49-63, American Geophysical Union, Geophysical Monograph 143.

Branca, S., Coltelli, M., De Beni, E., & Wijbrans, J. (2007). Geological evolution of Mount Etna volcano (Italy) from earliest products until the first central volcanism (between 500 and 100 ka ago) inferred from geochronological and stratigraphic data. *International Journal of Earth Sciences*, doi:10.1007/s00531-006-0152-0

Cannata, A., Catania, A., Alparone, S., & Gresta, S. (2008). Volcanic tremor at Mt. Etna: Inferences on magma dynamics during effusive and explosive activity. *J. Volcanol. Geotherm. Res.*, doi:10.1016/j.jvolgeores. 2007.11.027.

Cannata, A., Giudice, G., Gurrieri, S., Montalto, P., Alparone, S., Di Grazia, G., Favara, R., & Gresta, S. (2009a). Relationship between soil CO2 flux and volcanic tremor at Mt.

Etna: implications for magma dynamics. *Env. Earth Sci.*, doi:10.1007/s12665-009-0359-z.

Cannata, A., Hellweg, M., Di Grazia, G., Ford, S., Alparone, S., Gresta, S., Montalto, P., & Patanè, D. (2009b). Long period and very long period events at Mt. Etna volcano: Characteristics, variability and causality, and implications for their sources. *J. Volcanol. Geothherm. Res.*, 187, pp. 227–249.

Cannata, A., Montalto, P., Privitera, E., Russo, G. & Gresta, S. (2009c). Tracking eruptive phenomena by infrasound: May 13, 2008 eruption at Mt. Etna.-*Geophys. Res. Lett.*, 36, L05304, doi:10.1029/2008GL036738.

Cannata, A., Di Grazia, G., Montalto, P., Aliotta, M., Patanè, D., & Boschi, E. (2010). Response of Mount Etna to dynamic stresses from distant earthquakes. *J. Geophys. Res.*, 115, B12304, doi:10.1029/2010JB007487.

Cassinis, R., Finetti, I., Giese, P., Morelli, C., Steinmetz, L. & Vecchia, O. (1969). Deep seismic refraction research on Sicily. *Boll. Geof. Teor. Appl.*, 11, pp. 140-160.

Cardaci, C., Coviello, M., Lombardo, G., Patanè, G., & Scarpa, R. (1993). Seismic tomography of Etna Volcano. *J. Volcanol. Geotherm. Res.*, 56, pp. 357–368.

Catalano, R., Doglioni, C., & Merlini, S. (2001). On the Mesozoic Ionian basin. *Geophys. J. Int.*, 144, pp. 49-64.

Cernobori, L., Hirn, A., McBride, J.H., Nicolich, R., Petronio, L., Romanelli, M., & STREAMERS/PROFILES Working Groups (1996). Crustal image of the Ionian basin and its Calabrian margins. *Tectonophysics*, 264, 175-189.

Chiarabba, C., Amato, A., Boschi, E., & Barberi, F. (2000). Recent seismicity and tomographic modeling of the Mount Etna plumbing system. *J. Geophys. Res.*, 105, pp. 10923–10938.

Chiarabba, C., De Gori, P., & Patanè, D. (2004). The Mount Etna plumbing system: the contribution of seismic tomography. In *Mount Etna Volcano Laboratory*, Vol. 143, eds Bonaccorso, A., Calvari, S., Coltelli, M., Del Negro, C. & Falsaperla, S., American Geophysical Union Monography Series.

Chiocci, F.L., Coltelli, M., Bosman, A., & Cavallaro, D. (2011). Continental margin large-scale instability controlling the flank sliding of Etna volcano. *Earth Planet. Sci. Lett.*, doi:10.1016/j.epsl.2011.02.040.

Chouet, B., Page, R.A., Stephens, C.D., Lahr, J.C., & Power, J.A. (1994). Precursory swarms of long-period events at Redoubt Volcano (1989–1990), Alaska: their origin and use as a forecasting tool. *J. Volcanol. Geotherm. Res.*, 62, pp. 95–135.

Chouet, B. (1996). Long-period volcano seismicity: Its source and use in eruption forecasting. *Nature*, 380, pp. 309-316.

Chouet, B. (2003). Volcano seismology. *Pure Appl. Geophys.*, 160, pp. 739–788.

Chouet, B., Dawson, P., Ohminato, T., Martini, M., Saccorotti, G., Giudicepietro, F., De Luca, G., Milana, G. & Scarpa, R. (2003). Source mechanisms mechanisms of explosions at Stromboli Volcano, Italy, determined from moment□tensor inversions of very□long□period data. *J. Geophys. Res.*, 108(B1), 2019, doi:10.1029/2002JB001919.

Clemens, J.C., & Mawer, C.K. (1992). Granitic magma transport by fracture propagation. *Tectonophysics*, 204, pp. 339–360.

Colombi, B., Guerra, I., Luongo, G., & Scarascia, S. (1979). Profilo sismico a rifrazione Acireale-Termini Imerese. CNR Prog. Fin. Geodinamica, pub. 235, pp. 155-170, ed. Giannini, Napoli.

Coltelli, M., Del Carlo, P., & Vezzoli, L. (2000). Stratigraphic constraints for explosive activity in the last 100 ka at Etna volcano, Italy. *Int. J. Earth Sci.*, 89, pp. 665-677.

Continisio, R, Ferrucci, F., Gaudiosi, G., Lo Bascio, D., & Ventura, G. (1997). Malta escarpment and Mt. Etna; early stages of an asymmetric rifting process? Evidences from geophysical and geological data. *Acta Vulcanologica*, 9, 45-53.

De Barros, L., Bean, C., Lokmer, I., Saccorotti, G., Zuccarello, L., O'Brien, G., Métaxian, J.-P., Patanè, D. (2009). Source geometry from exceptionally high resolution long period event observations at Mt. Etna during the 2008 eruption. *Geophys. Res. Lett.*, 36, L24305, doi:10.1029/2009GL041273.

De Barros, L., Lokmer, I., Bean, C.J., O'Brien, G.S., Saccorotti, G., Métaxian, J.-P., Zuccarello, L., & Patanè, D. (2011). Source mechanism of long-period events recorded by a high-density seismic network during the 2008 eruption on Mount Etna. *J. Geophys. Res.*, 116, B01304, doi:10.1029/2010JB007629.

De Beni, E., Branca, S., Coltelli, M., Groppelli, G., & Wijbrans, J. (2011) – 40Ar/39Ar isotopic dating of Etna volcanic succession. In press in *It. J. Geosci.*

De Gori, P., Chiarabba, C., & Patanè, D. (2005). Qp structure of Mount Etna: Constraints for the physics of the plumbing system. *J. Geophys. Res.*, 110, B05303, doi:10.1029/2003JB002875.

De Luca, G., Filippi, L., Patanè, G., Scarpa, R., & Vinciguerra, S. (1997). Three dimensional velocity structure and seismicity of Mt. Etna volcano, Italy. *J. Volcanol. Geotherm. Res.*, 79, pp. 123– 138.

Di Grazia, G., Falsaperla, S., & Langer, H. (2006). Volcanic tremor location during the 2004 Mount Etna lava effusion. *Geophys. Res. Lett.*, 33, L04304. doi:10.1029/2005GL025177.

Di Grazia, G., Cannata, A., Montalto, P., Patanè, D., Privitera, E., Zuccarello, L., & Boschi, E. (2009). A new approach to volcano monitoring based on 4D analyzes of seismo-volcanic and acoustic signals: the 2008 Mt. Etna eruption. *Geophys. Res. Lett.*, 36, L18307, doi:10.1029/2009GL039567.

Doglioni, C., Innocenti, F., Mariotti, & G. (2001). Why Mt. Etna? *Terra Nova*, 13, pp. 25-31.

Falsaperla, S., Lanzafame, G., Longo, V., & Spampinato, S. (1999). Regional stress field in the area of Stromboli (Italy): insights into structural data and crustal tectonic earthquakes. *J. Volcanol. Geotherm. Res.*, 88, pp. 147-166.

Falsaperla, S., Alparone, S., D'Amico, S. , Di Grazia, G., Ferrari, F., Langer, H., Sgroi, T., & Spampinato, S. (2005). Volcanic tremor at Mt. Etna, Italy, preceding and accompanying the eruption of July–August, 2001. *Pageoph*, 162, pp. 1–22.

Froger, J.L., Merle, O., & Briole, P. (2001). Active spreading and regional extension at Mount Etna imaged by SAR interferometry. *Earth Planet. Sci. Lett.*, 148, pp. 245–258.

Gresta, S., Montalto, A., & Patanè, G. (1991). Volcanic tremor at Mt. Etna (January 1984–March 1985): its relationship to the eruptive activity and modelling of the summit feeding system. *Bull. Volcanol.*, 53, pp. 309–320.

Gresta, S., Peruzza, L., Slejko, D., & Distefano, G. (1998). Inferences on the main volcano-tectonic structures at Mt. Etna (Sicily) from a probabilistic seismological approach. *J. Seismol.*, 2, pp. 105– 116.

Gvirtzman, Z., Nur, A. (1999). The formation of Mount Etna as the consequence of slab rollback. *Nature*, 401, pp. 782–785.

Gudmundsson, A. (2006). How local stress control magma-chamber ruptures, dyke injections, and eruptions in composite volcanoes. *Earth Sci. Rev.*, 79, 1–31.

Hirn, A., Nercessian, A., Sapin, M., Ferrucci, F., & Wittlinger, G. (1991). Seismic heterogeneity of Mt. Etna: structure and activity. *Geophys. J. Int.*, 105, pp. 139– 153.

Hirn, A., Nicolich, R., Gallart, J., Laigle, M., & ETNASEIS Scientific Group (1997). Roots of Etna volcano in faults of great earthquakes. *Earth Planet. Sci. Lett.*, 148, pp. 171–191.

Kieffer, G. (1975). Sur l'existence d'une rift zone à l'Etna. *CR Acad Sci Paris*, 280, pp. 263-266.

Kieffer, G. (1985). Evolution structurale et dynamique d'un grand volcan polygénique: stades d'édification et activité actuelle de l'Etna (Sicile). *Thèse doctoral*, Université de Clermont-Ferrand, pp. 1-410.

Kumagai, H., Nakano, M., Maeda, T., Yepes, H., Palacios, P., Ruiz, M., Arrais, S., Vaca, M., Molina, I., & Yamashima, T. (2010). Broadband seismic monitoring of active volcanoes using deterministic and stochastic approaches. *J. Geophys. Res.*, 115, B08303, doi:10.1029/2009JB006889.

Kumazawa, M., Imanishi, Y., Fukao, Y., Furumoto, M., & Yamamoto, A. (1990). A theory of spectral analysis based on the characteristic property of a linear dynamic system. *Geophys. J. Int.*, 101, pp. 613-630.

Laigle, M., Hirn, A., Sapin, M., Lepine, J.C., Diaz, J., Gallart, J., & Nicolich, R. (2000). Mount Etna dense array local earthquake P and S tomography and implications for volcanic plumbing. *J. Geophys. Res.*, 105, pp. 21633– 21646.

Langer, H., & Falsaperla, S. (1996). Long-term observation of volcanic tremor on Stromboli Volcano (Italy): A synopsis. *Pageoph*, 147, pp. 57–82.

Lees, J.M., & Crosson, R.S. (1990). Bayesian ART versus conjugate gradient methods in tomographic seismic imaging: an application at Mount St. Helens, Washington. *Spatial Statistics and Imaging*: Proc. 1988 AMS-IMS-SIAM Summer Res. Conf., pp. 1–18.

Lentini, F., Carbone, S., & Guarnieri, P. (2006). Collisional and postcollisional tectonics of the Apenninic-Maghrebian orogen (southern Italy), in Dilek, Y., and Pavlides, S., eds., *Postcollisional tectonics and magmatism in the Mediterranean region and Asia*, Geological Society of America Special Paper 409, p. 57–81, doi:10.1130/2006.2409(04).

Lo Giudice, E., Patanè, G., Rasà, R., & Romano, R. (1982). The structural framework of Mount Etna. In: Romano R (ed) Mount Etna Volcano, a Review of Recent Earth Sciences Studies. *Memorie della Società Geologica Italiana*, 23, pp. 125-158.

Lo Giudice, E., & Rasà, A. (1992). Very shallow earthquakes and brittle deformation in active volcanic areas: the Etnean region as an example. *Tectonophysics*, 202, pp. 257-268.

Lokmer, I., Bean, C.J., Saccorotti, G., & Patanè, D. (2007). Moment-tensor inversion of LP events recorded on Etna in 2004 using constraints obtained from wave simulation tests. *Geophys. Res. Lett.*, 34, L22316, doi:10.1029/2007GL031902.

Lombardo, G., Coco, G., Corrao, M., & Gresta, S. (1996). Features of seismic events and volcanic tremor during the preliminary stages of the 1991–1993 eruption of Mt. Etna. *Ann. Geophys.*, 39, pp. 403–410.

Lundgren, P., Berardino, P., Coltelli,M., Fornaro, G., Lanari, R., Puglisi, G., Sansosti, E., & Tesauro, M. (2003). Coupled magma chamber inflation and sector collapse slip observed with SAR interferometry on Mt. Etna volcano. *J. Geophys. Res.*, 108, pp. 2247–2261.

Marsh, B. D. (2000). Magma Chambers. In *Encyclopedia of Volcanoes*, Sigurdsson, H., pp. 191-206, Academic Press.

Martinez-Arevalo, C., Patanè, D., Rietbrock, A., & Ibanez, J.M. (2005). The intrusive process leading to the Mt. Etna 2001 flank eruption: Constraints from 3-D attenuation tomography. *Geophys. Res. Lett*., 32, L21309, doi:10.1029/2005GL023736.

McGuire, W.J., Pullen, A.D. (1989). Location and orientation of eruptive fissures and feeder dykes at Mount Etna: influence of gravitational and regional stress regime. *J. Volcanol. Geotherm. Res*., 38, pp. 325-344.

McNutt, S.R. (1994). Volcanic Tremor Amplitude Correlated with Eruption Explosivity and its Potential Use in Determining Ash Hazards to Aviation. *U.S. Geological Survey Professional Paper*, 2047, pp. 377-385.

Monaco, C., Tapponnier, P., Tortorici, L., & Gillot, P.Y. (1997). Late Quaternary slip rates on the Acireale–Piedimonte normal faults and tectonic origin of Mt. Etna (Sicily). *Earth Planet. Sci. Lett.*, 147, pp. 125– 139.

Monaco, C., Catalano, S., Cocina, O., De Guidi, G.,Ferito, C., Gresta, S., Musumeci, C., & Tortorici, L. (2005). Tectonic control on the eruptive dynamics at Mt. Etna Volcano (Sicily) during the 2001 and 2002–2003 eruptions. *J. Volcanol. Geotherm. Res.*, 144, pp. 211-233.

Monteiller, V., Got, J.-L., Patanè, D., Barberi, G., & Cocina, O. (2009). Double-difference tomography at Mt Etna volcano: Preliminary results. In *The VOLUME Project. Volcanoes: Understanding Subsurface Mass Movement*, Bean, C. J., et al., pp. 74–84, VOLUME Consort./Jaycee, Dublin, Ireland.

Moran, S.C., Malone, S.D., Qamar, A.I., Thelen, W.A., Wright, A.K., & Caplan-Auerbach, J. (2008). Seismicity associated with the renewed dome-building eruption of Mount St. Helens 2004-2005. In *A volcano rekindled: the renewed eruption of Mount St. Helens, 2004-2006*, Sherrod, D.R., Scott, W.E., and Stauffer, P.H., chapter 2, U.S. Geological Survey Professional Paper.

Murray, J. B. (1990). High-level magma transport at Mount Etna volcano, as deduced from ground deformation measurements. In: *Magma Transport and Storage*, Ryan M.P., pp. 357–383, Wiley, Chichester.

Murru, M., Montuori, C., Wyss, M., & Privitera, E. (1999). The locations of magma chambers at Mt. Etna, Italy, mapped by b-values. *Geophys. Res. Lett.*, 26, pp. 2553–2556.

Neidell, N., & Taner, M.T. (1971). Semblance and other coherency measures for multichannel data. *Geophysics*, 36, pp. 482-497.

Neri, M., Acocella, V., & Behncke, B. (2004). The role of the Pernicana Fault System in the spreading of Mt. Etna (Italy) during the 2002–2003 eruption. *Bull. Volcanol.*, 66, pp. 417-430.

Neuberg, J. (2000). External modulation of volcanic activity. *Geophys. J. Int.*, 142, pp. 232–240.

Nicolich, R., Laigle, M., Hirn, A., Cernobori, L., & Gallart, J. (2000). Crustal structure of the Ionian margin of Sicily: Etna volcano in the frame of regional evolution. *Tectonoph.*, 329, pp. 121-139.

O'Brien, G.S., & Bean, C.J. (2004). A 3D discrete numerical elastic lattice method for seismic wave propagation in heterogeneous media with topography. *Geophys. Res. Lett*., 31, L14608, doi:10.1029/2004GL020069.

O'Brien, G. S., & Bean, C. J. (2009). Volcano topography, structure and intrinsic attenuation: Their relative influences on a simulated 3d viscoelastic wavefield. *J. Volcanol. Geotherm. Res.*, 183(1–2), 122–136.

Ohminato, T., Chouet, B., Dawson, P., & Kedar, S. (1998). Waveform inversion of very long period impulsive signals associated with magmatic injection beneath Kilauea Volcano, Hawaii. *J. Geophys. Res.*, 103, pp. 23839-23862.

Palano, M., Puglisi, G., & Gresta, S. (2008). Ground deformation patterns at Mt. Etna from 1993 to 2000 from joint use of InSAR and GPS techniques. *J. Volcanol. Geotherm. Res.*, 169, pp. 99-120.

Patanè, D., Chiarabba, C., Cocina, O., De Gori, P., Moretti, M., & Boschi, E. (2002). Tomographic images and 3D earthquake locations of the seismic swarm preceding the 2001 Mt. Etna eruption: Evidence for a dyke intrusion. *Geophys. Res. Lett.*, 29, 1497, doi:10.1029/2001GL014391.

Patanè, D., De Gori, P., Chiarabba, C., & Bonaccorso, A. (2003). Magma ascent and the pressurization of Mount Etna's volcanic system. *Science*, 299, pp. 2061-2063.

Patanè, D., Cocina, O., Falsaperla, S., Privitera, E., & Spampinato, S. (2004). Mt. Etna volcano: a seismological framework. In: S. Calvari, A. Bonaccorso, M. Coltelli, C. Del Negro and S. Falsaperla (Eds.), The Mt. Etna Volcano. AGU, Washington, D.C., 147−165.

Patanè, D., Mattia M. & Aloisi M., (2005). Shallow intrusive processes during 2002-2004 and current volcanic activity at Mt. Etna. *Geophys. Res. Lett.*, 32, L06302, 10.1029/2004GL021773.

Patanè, D., Barberi, G., Cocina, O., De Gori, P., & Chiarabba, C. (2006). Time-resolved seismic tomography detects magma intrusions at Mount Etna. *Science*, 313, pp. 821–823.

Patanè, D., Di Grazia, G., Cannata, A., Montalto, P., & Boschi, E. (2008). The shallow magma pathway geometry at Mt. Etna volcano. *Geochem. Geophys. Geosyst.*, 9, Q12021, doi:10.1029/2008GC002131.

Petford, N., Cruden, A.R. , McCaffrey, K.J.W., & Vigneresse, J.L. (2000). Granite magma formation, transport and emplacement in the Earth's crust. *Nature*, 408, pp. 669-673.

Rasà, R., Azzaro, R., & Leonardi, O. (1996). Aseismic creep on faults and flank instability at Mt. Etna volcano, Sicily. In: "Volcano Instability on the Earth and Other Planets", W.C. McGuire, A.P. Jones & J. Neuberg (ed.). Geological Society Special Publication 110, 179-192.

Rittmann, A. (1973). Structure and evolution of Mount Etna. *Philos. Trans. R. Soc. Lond.*, 274, 5-16.

Rust, D., & Neri, M. (1996). The boundaries of large-scale collapse on the flanks of Mount Etna, Sicily. In: *Volcano instability on the Earth and other planets*. McGuire, W.J., Jones, A.P., Neuberg, J., pp. 193–208, Geol. Soc. Lond. Spec. Pub. 110.

Rust, D., Behncke, B., Neri, M., & Ciocanel, A. (2005). Nested zones of instability in the Mount Etna volcanic edifice, Sicily. *J. Volcanol. Geotherm. Res.*, 144 , pp. 137–153.

Saccorotti, G., Lokmer, I., Bean, C., D. Grazia, G., & Patanè, D. (2007). Analysis of sustained long-period activity at Etna Volcano, Italy. *J. Volcanol. Geotherm. Res.*, 160, 340–354.

Selvaggi, G., & Chiarabba, C. (1995). Seismicity and P-wave velocity image of the Southern Tyrrhenian subduction zone. *Geophys. J. Int.*, 121, pp. 818 – 826.

Sharp, A.D.L., Davis, P.M., & Gray, F. (1980). A low velocity zone beneath Mount Etna and magma storage. *Nature*, 287, pp. 587-591.

Tanguy, J.C., Condomines, M., & Kieffer, G. (1997). Evolution of Mount Etna magma: constraints on the present feeding system and eruptive mechanism. *J. Volcanol. Geotherm. Res.*, 75, pp. 221– 250.

Tibaldi, A., & Groppelli, G. (2002). Volcano-tectonic activity along structures of the unstable NE flank of Mt. Etna (Italy) and their possible origin. *J. Volcanol. Geotherm. Res.*, 115, pp. 277-302.

Torelli, L., Grasso, M., Mazzoldi, G., & Peis, D. (1998). Plio-Quaternary tectonic evolution and structure of the Catania foredeep, the northern Hyblean Plateau and the Ionian shelf (SE Sicily). *Tectonophysics*, 298, pp. 209-221.

Varley, N., Arámbula-Mendoza, R., Reyes-Dávila, G., Stevenson, J., & Harwood, J. (2010). Long-period seismicity during magma movement at Volcán de Colima. *Bull. Volcanol.*, doi:10.1007/s00445-010-0390-7.

Vigneresse, J.L. (1999). Intrusion level of granitic massifs along the Hercynian belt: balancing the eroded crust. *Tectonophysics*, 307, pp. 277–295.

Withers, M., Aster, R., Young, C., Beiriger, J., Harris, M., Moore, S., & Trujillo, J. (1998). A comparison of select trigger algorithms for automated global seismic phase and event detection. *Bull. Seism. Soc. Am.*, 88, pp. 95-106.